Pathways to the Production of Precipitating Hydrometeors and Tropical Cyclone Development

J.-W. BAO

NOAA/Earth System Research Laboratory, Boulder, Colorado

S. A. MICHELSON AND E. D. GRELL

NOAA/Earth System Research Laboratory and Cooperative Institute for Research in Environmental Sciences, University of Colorado Boulder, Boulder, Colorado

(Manuscript received 15 October 2015, in final form 11 March 2016)

ABSTRACT

Pathways to the production of precipitation in two cloud microphysics schemes available in the Weather Research and Forecasting (WRF) Model are investigated in a scenario of tropical cyclone intensification. Comparisons of the results from the WRF Model simulations indicate that the variation in the simulated initial rapid intensification of an idealized tropical cyclone is due to the differences between the two cloud microphysics schemes in their representations of pathways to the formation and growth of precipitating hydrometeors. Diagnoses of the source and sink terms of the hydrometeor budget equations indicate that the major differences in the production of hydrometeors between the schemes are in the spectral definition of individual hydrometeor categories and spectrum-dependent microphysical processes, such as accretion growth and sedimentation. These differences lead to different horizontally averaged vertical profiles of net latent heating rate associated with significantly different horizontally averaged vertical distributions and production rates of hydrometeors in the simulated clouds. Results from this study also highlight the possibility that the advantage of double-moment formulations can be overshadowed by the uncertainties in the spectral definition of individual hydrometeor categories and spectrum-dependent microphysical processes.

1. Introduction

Clouds are an essential meteorological element in tropical cyclones (TCs) because as a cluster of convective entities, they must become organized around a central area of surface low pressure for a TC to form and develop. In fact, the energy required for a TC to intensify comes from the direct transfer of sensible heat and latent heat from the warm ocean surface upward via convection. Clouds associated with TCs are typically organized into large rings and bands, which have cloud and precipitation structures similar to the mesoscale convective systems outside of the tropics [see the comprehensive review of these clouds by Houze (2010)]. Therefore, similar to the problem of improving numerical weather prediction (NWP) models for quantitative precipitation forecasts outside the tropics, the problem of improving numerical TC forecasts is closely related to how to better simulate the net effects of clouds on model-resolved winds, temperature, and moisture.

Although TCs are among the most important weather phenomena in the tropics, model skill at predicting TC track and intensity has not always been satisfactory. It has been widely recognized that errors in NWP model initialization, including the vortex initialization pertinent to TCs, are a major factor contributing to the forecast errors in the tropics [see Davidson et al. (2014), and references therein]. It has also become clear that uncertainties in the model physics in simulating dynamical processes essential to the development of clouds in TCs are another major factor that hinders the improvement of model-based TC prediction (Bao et al. 2012). In particular, uncertainties in the parameterizations of cold rain processes, such as cloud ice nucleation, greatly influence the accuracy of NWP models, not only in TC intensity, but also in TC track and structure (Jin et al. 2014).

Denotes Open Access content.

Corresponding author address: Jian-Wen Bao, NOAA/ESRL, 325 Broadway, Boulder, CO 80305.
E-mail: jian-wen.bao@noaa.gov

DOI: 10.1175/MWR-D-15-0363.1

As both research and operational NWP models are run at progressively finer horizontal and vertical resolutions, experiments with more complex microphysical parameterization (MP) schemes are being used for TC prediction. These models can explicitly simulate complex dynamical and microphysical processes associated with deep, precipitating convection in TCs. However, there remain questions about the numerical behavior of the explicit cloud simulations, such as how quantitative aspects of model-simulated clouds are affected as the model resolution increases if the cloud physics parameterization schemes are unchanged. More importantly, whether or not the model solution with a given physics configuration will eventually converge as the model resolution continues increasing is still a subject of research. Addressing this problem is not straightforward, given that there are more than a few competing MP schemes commonly used in TC forecast and research models, as exemplified in the Weather Research and Forecasting (WRF) Model (Skamarock et al. 2008). Nevertheless, as indicated in the sensitivity study carried out by Bao et al. (2012), there is a need for the modeling community to address the question as to what are the fundamental differences in various MP schemes that lead to the differences in the simulated intensity and structural evolution of TCs.

Differences in the MP schemes lead to different meteorological outcomes from NWP models in which these schemes are applied. For example, as often discussed in the literature, differences in the parameterized production rates of hydrometeors are the major reason for the sensitivity of the quantitative precipitation forecast (QPF) to different microphysics schemes (see, e.g., Gallus and Pfeifer 2008; Reeves and Dawson 2013). Despite the vast and growing literature on the subject of microphysics parameterizations, there is no consensus as to what constitutes the minimal complexity in a MP scheme for an operational model to reasonably reproduce measurable aspects of TC development, as well as to provide an accurate QPF for land-falling TC events. It is foreseeable that significant convergence of parameterizations of cloud microphysical processes will not happen soon since there are still gaps in both theoretical and empirical descriptions of cloud microphysical processes due to the lack of sufficient knowledge on the natural variability of cloud/hydrometeor and aerosol distributions, and the complex interaction of various microphysical processes. Filling these gaps will take efforts in basic research and well-coordinated field programs to obtain the detailed microphysical observations required for validating parameterization schemes.

The main objective of this study is to investigate how sensitive the WRF Model is to uncertainties in parameterizations of cloud microphysical processes in the

TABLE 1. Summary of hydrometeor size distributions in the WSM6 and THOM schemes. Mass distribution: $m_x(D) = a_{mx}D_x^{b_{mx}}$, number distribution: $N_x = N_{0x}D_x^{P_x}\exp(-\lambda_x D_x)$, and fall speed distribution: $V(D) = a_{vx}D_x^{b_{vx}}\exp(-\gamma_x D)$.

Scheme	Species	Assumed distribution	N_{0x} (m^{-4})	a_{mx} ($\mathrm{kg\,m}^{-b_{mx}}$)	b_{mx}	a_{vx} ($\mathrm{m\,s}^{-1}\,\mathrm{m}^{-b_{vx}}$)	b_{vx}	ρ_x ($\mathrm{kg\,m}^{-3}$)	γ_x	P_x
WSM6	Cloud	Exponential	300×10^6	$\pi\rho_r/6$	3	—	—	1000	0.0	0.0
	Rain	Exponential	8×10^6	$\pi\rho_r/6$	3	841.9	0.8	1000	0.0	0.0
	Snow	Exponential	Temperature dependent (Houze et al. 1979)	$\pi\rho_s/6$	3	11.72	0.41	100	0.0	0.0
	Graupel	Exponential	4×10^6	$\pi\rho_g/6$	3	330	0.8	500	0.0	0.0
	Ice[a]	Exponential	—	—	—	—	—	—	—	—
THOM	Cloud	Gamma	100×10^6	$\pi\rho_c/6$	3	0.0	0.0	1000	195.0	$\mathrm{Min}(15, 10^9/N_{0c} + 2)$
	Rain	Exponential	Prognostic	$\pi\rho_r/6$	3	4854.4	1	1000	195.0	0.0
	Ice	Exponential	Prognostic	$\pi\rho_i/6$	3	1847.5	1	890	0.0	0.0
	Snow	Exponential + gamma	Temperature dependent (Field et al. 2005)	0.069	2	40	0.55	100	100.0	0.636
	Graupel	Exponential	$\max\left[10^4, \min\left(\frac{200}{q_g}, 5 \times 10^6\right)\right]$	$\pi\rho_g/6$	3	442	0.89	400	0.0	0.0

[a] The distribution functions for cloud ice in the WSM6 scheme are significantly different from the THOM scheme. In the WSM6 scheme, the total number mixing ratio of cloud ice is expressed as a function of cloud ice mixing ratio q_i, given by $N_i = c(\rho_{\mathrm{air}}q_i)^d$, where c and d are constants. The mass-weighted fall speed V_i is expressed similarly.

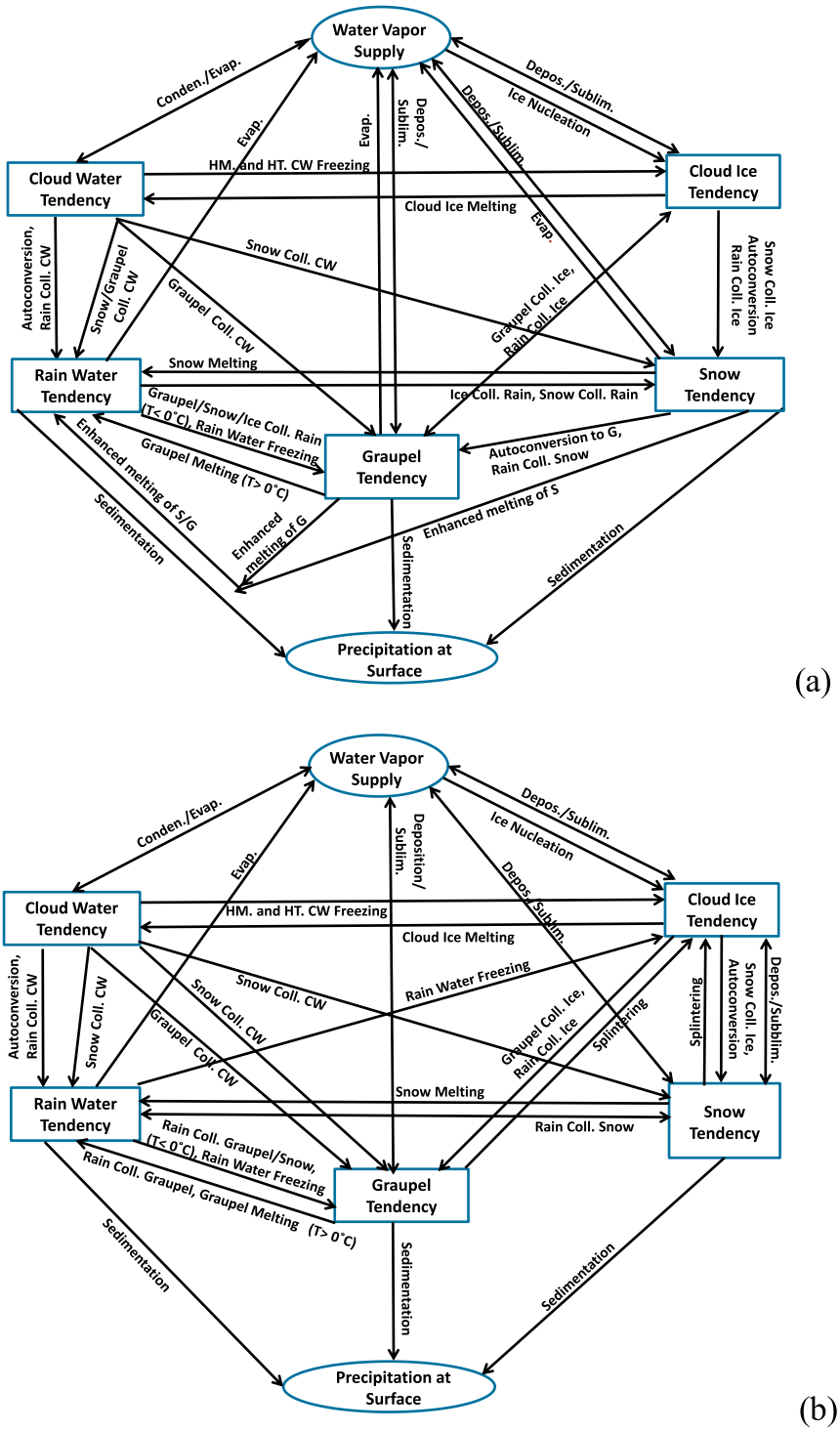

FIG. 1. Flowchart diagram of all the microphysical processes of the cloud water, rainwater, cloud ice, snow, and graupel tendency equations in (a) the WSM6 and (b) the THOM schemes. The process of slow cloud ice sedimentation existing in both schemes is omitted in the diagram.

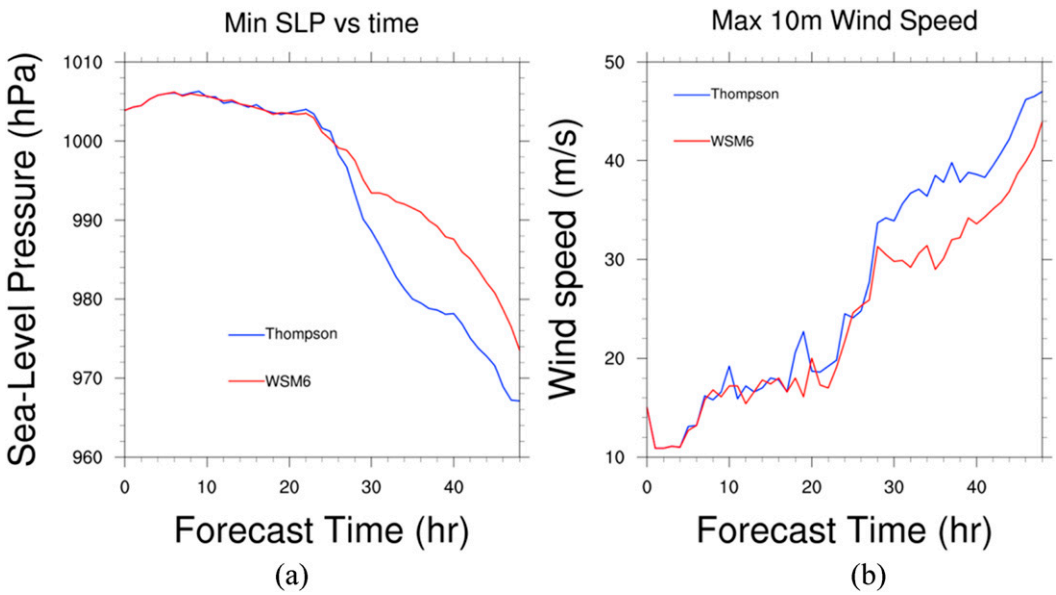

FIG. 2. Time series of the (a) minimum sea level pressure (hPa) and (b) the maximum 10-m wind speed (m s^{-1}). The red lines are for the WSM6 run, while the blue lines are for the THOM run.

intensification of a TC by addressing the following two questions: 1) What are the major microphysical processes affecting the simulated initial rapid intensification? 2) How do the microphysics parameterization schemes used in this study differ fundamentally in the parameterizations of these processes? Answering these questions will scientifically provide insight into the feedback mechanisms of microphysical processes contributing to TC intensification, in addition to the well-known mechanism of latent heat release through phase change in the formation and growth of cloud hydrometeors. It will also provide useful information as to what meteorological observations can be used to validate parameterized cloud microphysical processes. To this end, the sensitivity of an idealized TC intensification as simulated by the WRF Model to two different MP schemes is first shown in terms of the maximum surface wind, the minimum sea level pressure, and the azimuthally averaged structure of the simulated TC. Then, the sensitivity of the idealized TC intensification to the two MP schemes is investigated through the budget analysis of the microphysical terms in the hydrometeor prognostic equations. Also, by examining the impact of hydrometeor production and precipitation rates on the simulated TC intensification, further insight and understanding of the effects of microphysical processes on TC development are gained.

The rest of the paper is organized as follows: the setup of the WRF sensitivity experiments and the two MP schemes investigated in this study is summarized in section 2. The results from both experiments are presented and compared in section 3. Summary and discussion of the results are provided in section 4, along with their implications for TC model evaluation.

2. Overview of the WRF Model setup and two MP schemes

a. Model description and experiment design

The sensitivity experiments presented here are run using version 3.5 of the WRF Model (Skamarock et al. 2008) with a parent domain at a horizontal resolution of 9 km with a single nonmoving nest at 3-km horizontal resolution. The outer 9-km grid has 481 × 481 grid points, while the 3-km grid has 241 × 241 grid points. There are a total of 43 vertical levels with the model top at 50 hPa. To initialize the WRF Model with an idealized vortex, the nonlinear balance equation in the pressure-based sigma coordinate system described in Wang (1995) is solved within the WRF-grid framework on an f plane located at 12.58°N. The mass field is derived from the wind field corresponding to an axisymmetric cyclonic vortex of maximum surface tangential wind set to 15 m s^{-1} at 90 km from the vortex center embedded in a quiescent flow. The far-field temperature and humidity are based on Jordan's Caribbean sounding (Gray et al. 1975). In both experiments, the sea surface temperature (SST) was set to 302 K.

To assess the impact of variations in the parameterized microphysical processes on the development of simulated TCs, idealized simulations are performed using two MP schemes available in the WRF Model with

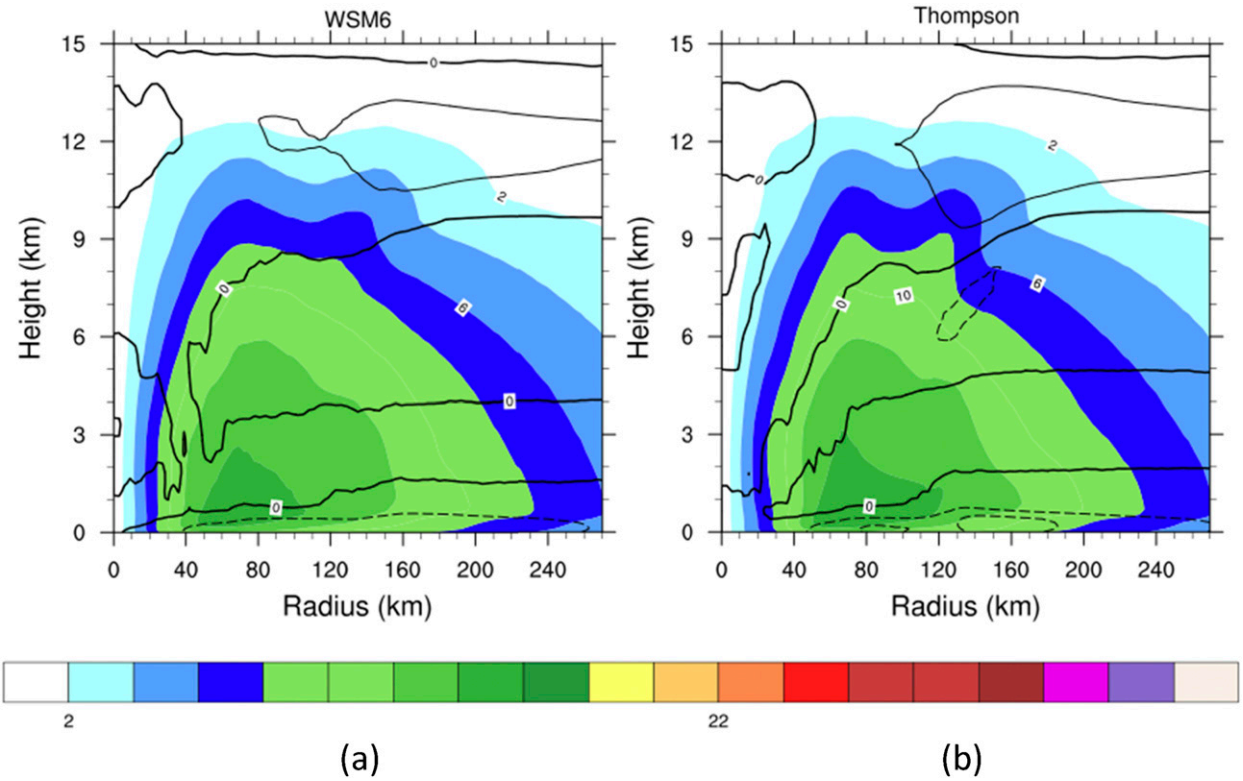

FIG. 3. Azimuthally averaged tangential wind speed (color shaded, 2 m s^{-1} interval) and radial wind speed (black contours, 2 m s^{-1} interval, negative values are dashed) averaged from 1 to 24 h into the simulation for (a) the WSM6 and (b) the THOM runs.

varying complexity. In order of increasing complexity, these are the WRF single-moment 6-class scheme (WSM6; Hong and Lim 2006) and the hybrid (double-moment cloud ice and rain) scheme by Thompson et al. (2008; hereafter referred to as THOM). Additionally, the Mellor–Yamada–Janjić schemes for the surface layer and planetary boundary layer are used to parameterize the flux transport and the subsequent mixing in the atmosphere. The surface forcing is prescribed using the aforementioned constant SST. No convective parameterization scheme is used on either domain. The Rapid Radiative Transfer Model (RRTM) longwave radiation scheme (Mlawer et al. 1997) and the shortwave radiation scheme of Dudhia (1989) are used to simulate the radiative forcing.

b. Size-dependent microphysical parameterizations

In MP schemes commonly used in NWP models, it is generally assumed that the size distribution of each hydrometeor class has the form of a complete gamma distribution:

$$N_x = N_{0x} D_x^{P_x} \exp(-\lambda_x D_x),$$

where N_x is the number of hydrometeor particles per unit volume (i.e., number concentration) per unit size range at diameter D_x of hydrometeor x (denoting the hydrometeor type, i.e., $c, r, i, s,$ or g for cloud water, rainwater, cloud ice, snow, or graupel, respectively); and P_x, N_{0x}, and λ_x are the spectral index, intercept, and slope of the size distribution, respectively. In the two MP schemes employed in this study, it is assumed that $P_x = 0$, which means the distribution is a simple exponential function with the largest concentrations at the smallest sizes. Both N_{0x} and λ_x can be written in terms of the mass mixing ratio q_x and the total number concentration N_{Tx}:

$$\lambda_x = \left[\frac{a_{mx} N_{Tx} \Gamma(P_x + b_{mx} + 1)}{\rho_a q_x \Gamma(P_x + 1)}\right]^{1/b_{mx}},$$

$$N_{0x} = \frac{N_{Tx} \lambda_x^{P_x+1}}{\Gamma(P_x + 1)},$$

where Γ is the Euler gamma function, ρ_a is air density, and the parameters a_{mx} and b_{mx} are empirical constants and given by the assumed power-law mass–diameter (m–D) relationship of the hydrometeors for each species x, where $m_x = a_{mx} D_x^{b_{mx}}$. Associated with the above size distribution, fall speeds of each species are given by

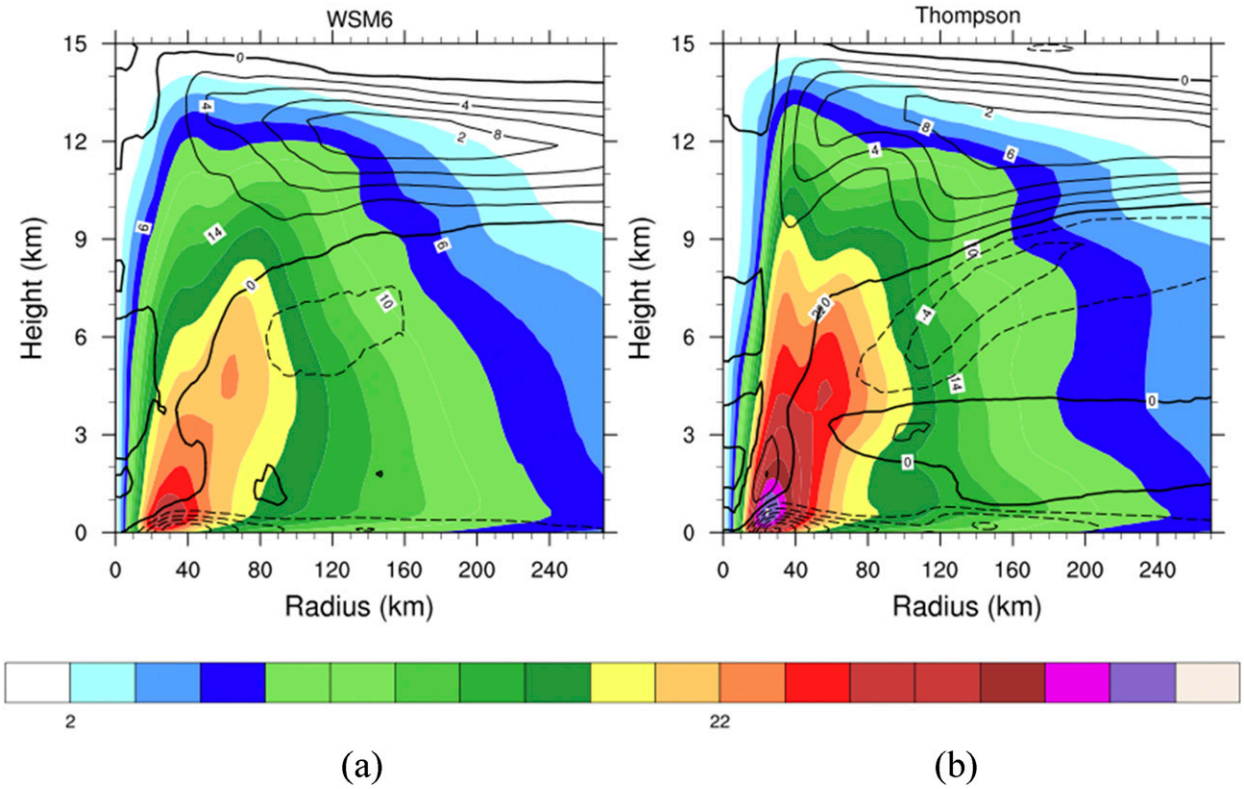

FIG. 4. As in Fig. 3, but for the average from 25 to 36 h into the simulations.

$$V_x = \frac{a_{vx}\Gamma(b_{mx} + b_{vx} + 1)}{\lambda_x^{b_{vx}}\Gamma(b_{mx} + 1)},$$

where the parameters a_{vx} and b_{vx} are empirical constants obtained from observed velocity–diameter relations.

In general, both single-moment and double-moment MP schemes utilize the aforementioned spectral relations in the prediction of the evolution of a mass mixing ratio q_x and allow for the hydrometeors' size distribution to evolve with time. However, in single-moment schemes, N_{0x} is assumed to be constant or diagnosed from other prognostic model variables such as temperature, and therefore N_x is constrained only by q_x, which does not allow for observed behaviors such as size sorting or aggregation (see, e.g., Milbrandt and Yau 2005; Van Weverberg et al. 2012). In double-moment schemes, the integral of the size distribution N_x (i.e., N_{Tx}) is predicted along with q_x, hence prescribing and diagnosing the intercept parameter N_{0x} is no longer necessary (Ferrier 1994; Seifert and Beheng 2006; Morrison et al. 2009). All hydrometeors settle at a mass-weighted mean fall speed in the prognostic equations for mass, though the number concentrations of hydrometeors in double-moment schemes have a different fall speed than the mass. For comparison, the parameters used in size distribution, mass, and fall speed specifications in the two MP schemes used in this study are summarized in Table 1. While the WSM6 scheme only predicts one moment, the mass mixing ratio q for each hydrometeor (and number concentration is diagnosed from q following a power law), the THOM scheme additionally explicitly predicts number concentration for cloud ice and rainwater.

c. *Pathways to precipitation production in the WSM6 and THOM schemes*

Figure 1 depicts how the interaction of prognostic mass mixing ratios of water vapor, cloud water, cloud ice, rainwater, snow, and graupel leads to precipitation at the surface. (The sources and sinks of each prognostic mass mixing ratio are described in Tables 2–6.) In both the WSM6 and THOM schemes, using the definition widely used in the literature (see, e.g., Cotton et al. 2010), clouds are categorized as warm, cold, or mixed phase, depending on whether the phase of the hydrometeors in the clouds is liquid, solid, or a mixture of liquid and solid. In warm clouds, liquid cloud drops interact to produce precipitation. Analogously, clouds consisting entirely of frozen hydrometeors are defined as cold clouds. While ice is a necessary component of the cold-cloud process, the liquid phase still plays important

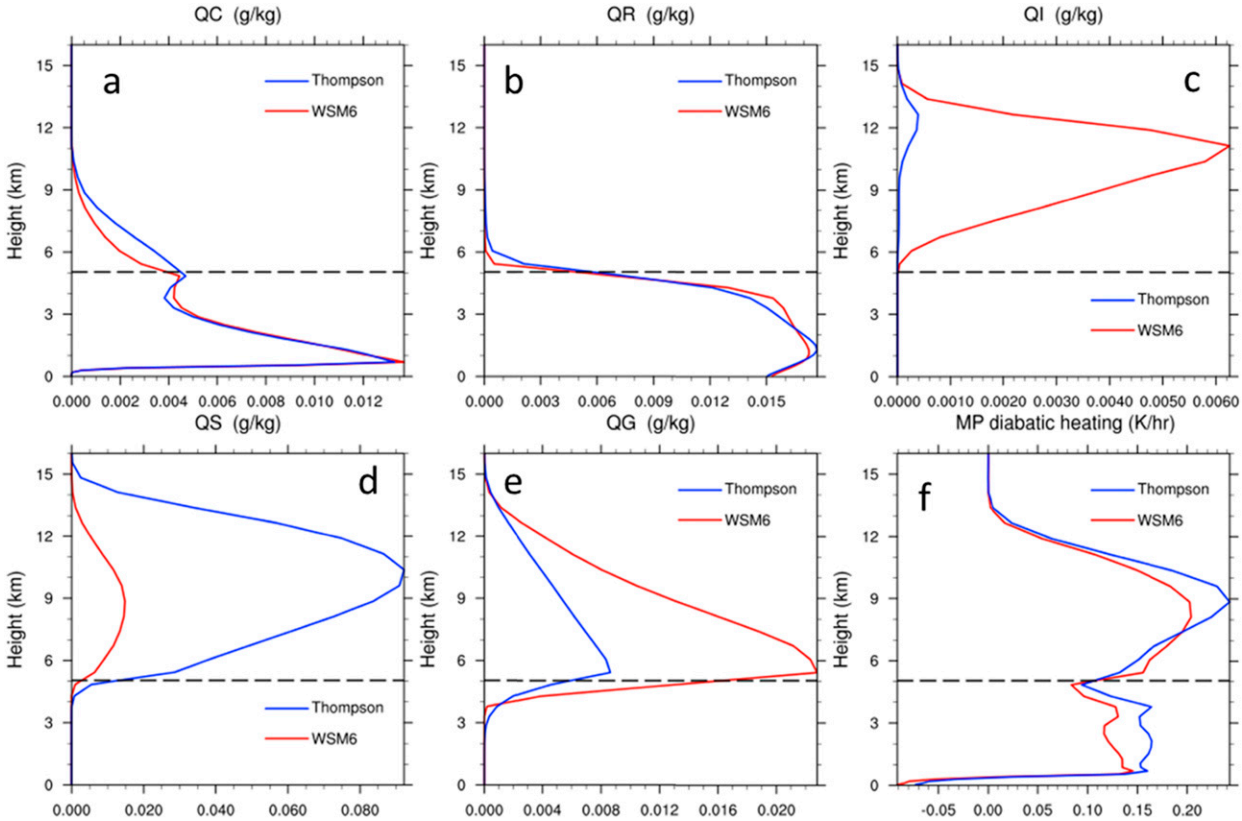

FIG. 5. Domain- and time-averaged (1–24 h) vertical distributions of mass mixing ratios (g kg^{-1}) of (a) cloud water, (b) rainwater, (c) cloud ice, (d) snow, and (e) graupel. (f) The diabatic heating profile due to the microphysics. The blue lines are from the THOM run and the red lines are from the WSM6 run. The black dashed line is the 0°C line.

roles in the evolution of the ice phase in many deep clouds associated with TC development. This is because convective clouds easily extend into air colder than about −10°C and supercooled droplets may coexist with frozen hydrometeors to form mixed-phase clouds until temperatures are cold enough to support homogeneous freezing at or below −40°C. From Fig. 1 it is clear that both schemes include most of the same parameterized processes, particularly in the warm phase. It is in the cold and mixed-phase interactions where the primary process differences between the schemes occur.

Although there are obvious numerical differences in the size distribution of cloud water droplets and the treatment of warm rain processes in the two schemes, there are no fundamental differences in their pathway to the production of cloud water through condensation, which occurs only when water vapor exceeds the same saturation threshold in both the WSM6 and THOM schemes. However, the WSM6 scheme uses a simple saturation adjustment procedure (cf. Reisner et al. 1998) for cloud water condensation, while the THOM scheme uses a more accurate Newton–Raphson iterative technique (Langlois 1973) to solve the Clausius–Clapeyron equation. Both schemes have the same warm-phase pathways to the formation of rainwater. That is, condensation of water vapor forms cloud water, which is then collected by large drops, which originate from the initial coalescence growth of cloud water, to form raindrops that are large enough to precipitate. This collision–coalescence process also forms the supercooled drops that enhance cloud glaciation and contribute to the production of frozen precipitation. Rainwater in the WSM6 scheme evaporates first and then cloud water evaporates if the air is still subsaturated, while in the THOM scheme, cloud water evaporates first and then rainwater evaporates only if subsaturated conditions remain. Vapor depositional growth of rainwater is ignored in both schemes since the saturation adjustment scheme will remove any supersaturation with respect to water by increasing the cloud water content instead of rain.

The main pathway to the production of frozen precipitation in the two schemes conceptually involves multiple processes. Cloud ice can either form from supersaturated vapor at subfreezing temperatures (as with

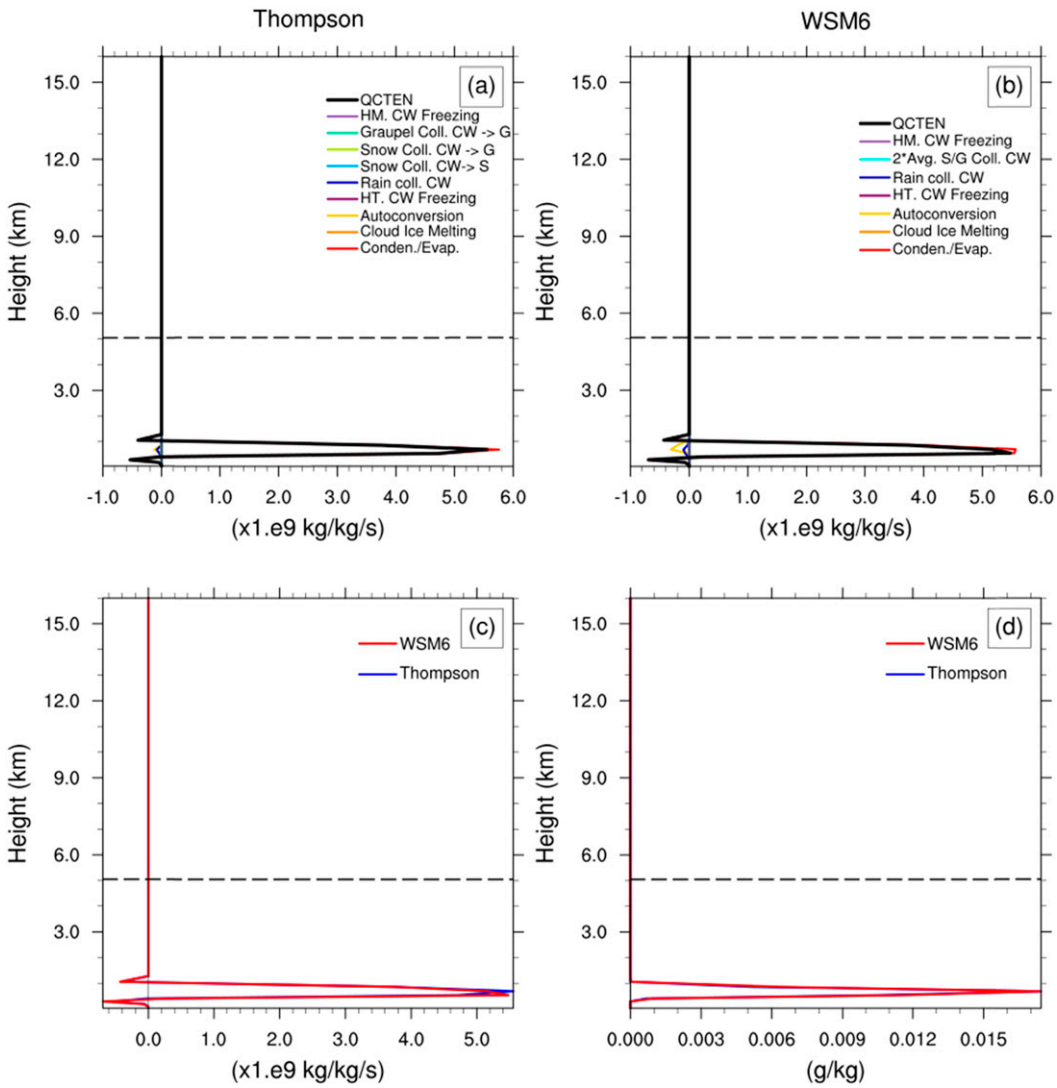

FIG. 6. The vertical profiles of the domain average of the cloud water mass mixing ratio tendency budget (scaled by 10^9) for (a) the THOM and (b) the WSM6 runs at forecast hour 4. The legends are explained in Table 2. The vertical profiles of the domain average of (c) the cloud water mass mixing ratio tendency (scaled by 10^9) and (d) the cloud water mass mixing ratio (in both, the red line is the WSM6 run and the blue line is the THOM run). The black dashed line is the 0°C line.

deposition nucleation) or from supercooled liquid (homogeneous/heterogeneous freezing nucleation). Vapor depositing onto small cloud ice crystals may cause them to grow large enough to sediment and begin colliding with other crystals. Aggregation of the ice crystals leads to snowflakes that may fall below the freezing level where they melt and fall out as rain. In deep convective clouds, snowflakes may also collect supercooled cloud water to form graupel. The growth of graupel by the collection of supercooled cloud water (a process referred to as riming) is key to an effective cold-precipitation process in some convective storms, as well as contributing to the glaciation and electrification of clouds in general (Lamb 2001). Since graupel-type hydrometeors are several hundred micrometers in radius, the riming process becomes an efficient way to convert condensate into precipitation-sized particles if there is an abundant supply of supercooled cloud water, which is a typical situation associated with tropical deep convective clouds (Houze 2010).

There are significant differences between the WSM6 and THOM schemes in their assumed pathways to the production of frozen hydrometeors. The WSM6 scheme allows new crystals to nucleate when supersaturation

TABLE 2. Terms in the cloud water mass mixing ratio budget, used in the legends of Figs. 6, 7, and 9. Actual variable names in the WRF code, where applicable, are also included in parentheses.

Legend name in THOM	Legend name in WSM6	Description
QCTEN	QCTEN	Cloud water mass mixing ratio tendency
HM. CW freezing (pri_ifz)	HM. CW freezing (pihmf)	Homogeneous freezing of cloud water to cloud ice ($T < -40°C$)
Graupel coll. CW→ G (prg_gcw)	2*Avg S/G coll CW (paacw)	Collection of cloud water by snow and graupel
Snow coll. CW → G (prg_scw)		THOM: Legends indicate the species formed
Snow coll. CW → S (prs_scw)		WSM6: If $T < 0°C$, snow and graupel are formed; if $T \geq 0°C$ rain is formed
Rain coll. CW (prr_rcw)	Rain coll. CW (pracw)	Rain collecting cloud water to form rain
HT. CW freezing (pri_wfz)	HT. CW freezing (pihtf)	Heterogeneous freezing of cloud water to form cloud ice ($-40° \leq T < -0°C$)
Autoconversion (prr_wau)	Autoconversion (praut)	Autoconversion of cloud water to rainwater
Cloud ice melting (prw_iml)	Cloud ice melting (pimlt)	Instantaneous melting of cloud ice to cloud water
Conden./evap. (prw_vcd)	Conden./evap. (pcond)	Cloud water condensation and evaporation

with respect to ice is achieved at any level where the temperature is below 0°C, while the THOM scheme additionally requires that a supersaturation of 25% be reached before nucleation starts. The WSM6 scheme diagnoses the total number mixing ratio of cloud ice from its mass mixing ratio while in the THOM scheme it is prognostic. Both schemes include a size threshold to separate cloud ice and snow. In the THOM scheme, this size threshold is 300 μm while in the WSM6 scheme it is 500 μm. The physical meaning of this threshold is twofold: the mean sizes of cloud ice particles are defined differently between the two schemes, and the THOM scheme more readily converts ice particles into the snow species than the WSM6 scheme.

In both the WSM6 and THOM schemes, snow by definition is assumed to be made up of clusters or aggregates of small ice crystals and to be produced by collision and coalescence among small ice crystals. It is also assumed in both schemes that small ice crystals can grow to snow size by vapor deposition that releases the latent heat of sublimation. Another pathway to the production of snow species in both schemes is through riming, in which small cloud ice crystals become large enough to sediment through a population of supercooled cloud droplets, then collide and coalesce with them. This riming growth process, unlike the growth of a hydrometeor species through the collision and coalescence of hydrometeors of the same phase, results in latent heat release. In both schemes, such a riming process not only serves as a pathway to the production of snow, but also as a pathway to the production of graupel. In addition to riming, the two schemes also produce graupel through freezing of liquid raindrops and through the collection of snow and ice by rainwater.

Despite the fact that the two schemes have similar conceptualized processes responsible for frozen hydrometeor production, there is no a priori information available in the literature about whether or not the quantitatively dominant pathways to the production of a particular frozen hydrometeor between the two schemes are similar. Given that the different size distributions of hydrometeors in the two schemes affect all the parameterized size-dependent processes quantitatively, it is important to discern how the two schemes are different in their individual pathways to the production of frozen hydrometeors.

3. Results

a. *Sensitivity of TC intensification and structure*

A comparison of time series of the minimum sea level pressure (PMIN) and maximum 10-m wind speeds (VMAX) from the two model runs using the WSM6 and THOM schemes is shown in Fig. 2. Differences between the two runs in terms of both PMIN and VMAX are not very discernable until 24 h into the simulations. After 24 h, the intensity of the simulated TC vortex is greater in the THOM run than the WSM6 run, as measured by both PMIN and VMAX. Figure 3 depicts azimuthally averaged tangential and radial wind speeds, averaged from 1 to 24 h into the simulations, the gestation period after which the simulated vortex starts to systematically intensify. The maximum average radial winds are slightly greater in the THOM run than the WSM6 run, indicating the simulated TC vortex intensity is overall slightly stronger in the THOM run than the WSM6 run during the first 24 h of the simulations. As shown in Fig. 2, the differences in the intensity grow significantly after 24 h, particularly during the time window between 25 and 36 h. Consistently, differences in the vortex structure grow as well. Azimuthally averaged tangential wind speed and radial wind speed (Fig. 4) show that the boundary layer inflow is stronger in the THOM run than

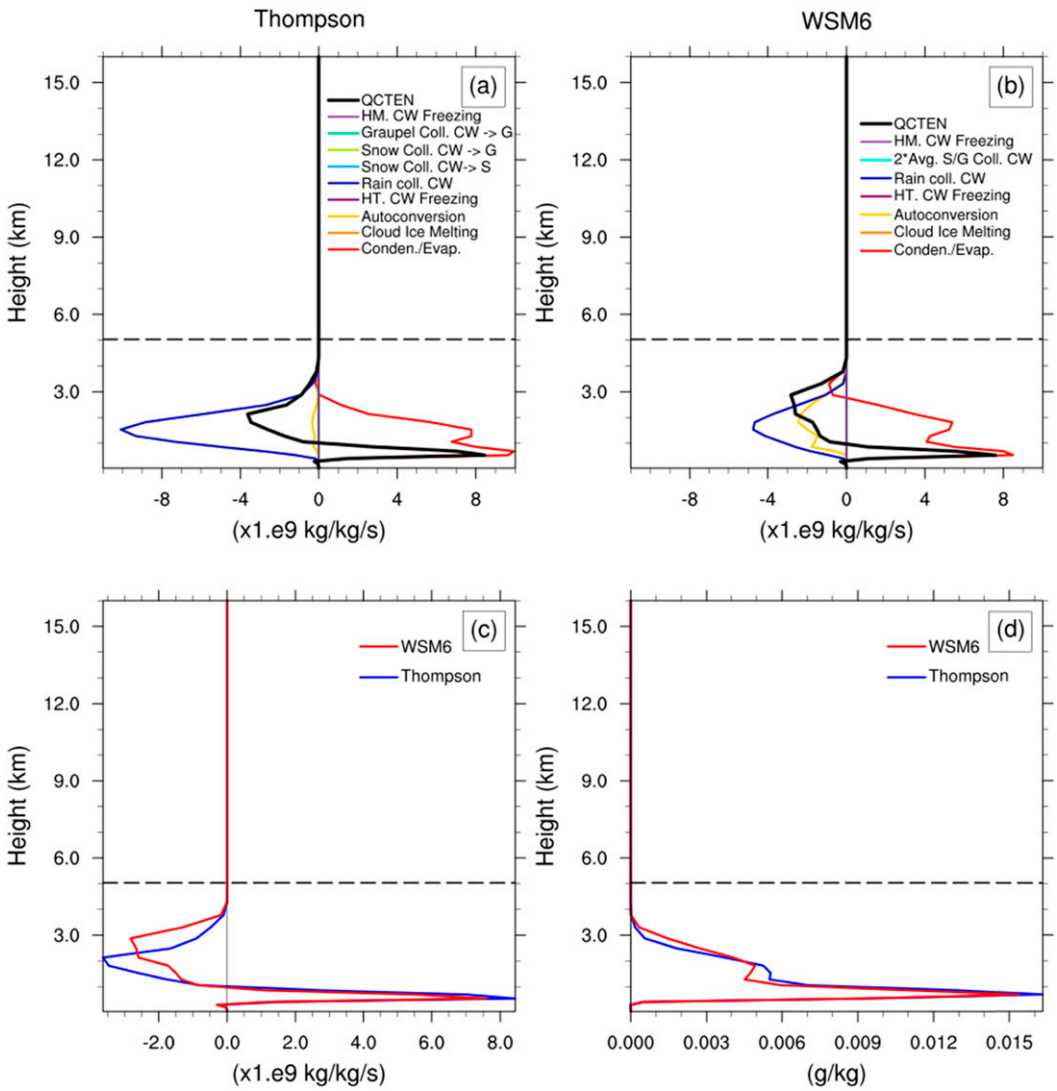

FIG. 7. As in Fig. 6, but at forecast hour 5.

in the WSM6 run during 25–36 h. Above this boundary layer inflow, there is prominent outflow in the THOM run, but not in the WSM6 run. There is also stronger midlevel inflow in the THOM run than the WSM6 run, which is consistent with the difference in the latent heating profiles (shown in Fig. 5f). The maximum tangential winds in the THOM run are greater than the WSM6 run. Also, the axis of strong winds ($>25\,\mathrm{m\,s^{-1}}$) in the THOM run extends nearly vertically upward, while it is more tilted in the WSM6 run. Corresponding to a stronger vortex, the THOM run produces a warmer core than the WSM6 run (not shown). However, there is not much difference in the radius of maximum surface winds between the two runs (both being around 25 km). To test the robustness of the aforementioned difference in the simulated TC intensification associated with the idealized environment, two additional sets of runs are carried out in which the relative humidity of the initial sounding is perturbed by ±5% and ±7.5% for each scheme. The results from these runs indicate that the THOM scheme consistently produces a greater intensity than the WSM6 scheme (not shown).

The difference in the intensity between the THOM and WSM6 runs is related to the difference in the conversion of latent heat energy that is acquired from the underlying ocean through evaporation and is released in the atmosphere through the production of cloud hydrometeors. Figure 5 shows the domain-averaged vertical profiles of the mass mixing ratios of cloud water, rainwater, cloud ice, snow, and graupel, along with the diabatic heating from the THOM and WSM6 runs averaged over 1–24 h into the simulations. During this time

TABLE 3. Terms in the rainwater mass mixing ratio budget equation, used in the legends of Figs. 8 and 10. Actual variable names in the WRF code, where applicable, are also included in parentheses.

Legend name for THOM	Legend name for WSM6	Description
QRTEN	QRTEN	Rainwater mass mixing ratio tendency
Sedimentation	Sedimentation	Sedimentation of rainwater
Evap. (prv_rev)	Evap. (prevp)	Evaporation of rainwater
Rain water freezing → I (pri_rfz)		Freezing of rain drops to form cloud ice
Rain water freezing → G (prg_rfz)	Rain water freezing → G (pgfrz)	Freezing of rain drops to form graupel
Graupel melting (prr_gml)	Graupel melting (pgmlt)	Graupel melting to form rainwater
Snow melting (prr_sml)	Snow melting (psmlt)	Snow melting to form rainwater
Rain coll. ice (prr_rci)	Rain coll. ice (piacr)	Rain collecting ice to form snow or graupel in WSM6, but only graupel in THOM, for $T < 0°C$
Rain coll. graupel (prr_rcg)		Rain collecting graupel to form larger graupel ($T < 0°C$) or rainwater ($T \geq 0°C$)
Rain coll. snow (prr_rcs)		For $T < 0°C$, rain collecting snow to form snow; for $T \geq 0°C$, to form rain
	Graupel coll. rain (pgacr)	Graupel collecting rain to form larger graupel ($T < 0°C$) or to form rain as part of enhanced melting of snow ($T \geq 0°C$)
	Snow Coll. Rain (psacr)	Snow collecting rain to form snow or graupel for $T < 0°C$; for $T \geq 0°C$, to form rain as part of enhanced melting of snow
Rain Coll. CW (prr_rcw)	Rain Coll. CW (pracw)	Rain collecting cloud water to form rainwater
Autoconversion (prr_wau)	Autoconversion (praut)	Autoconversion of cloud water to rainwater
	Enhanced melting of G (pgeml)	Enhanced melting of graupel by accretion of rainwater
	Enhanced melting of S (pseml)	Enhanced melting of snow by accretion of rainwater
	2*Avg. S/G Coll. CW (paacw)	Averaged snow and graupel collecting cloud water to form rain for $T \geq 0°C$, and snow and graupel for $T \leq 0°C$

period, both runs have similar vertical distributions of cloud and rainwater. The greatest differences are in the vertical distributions of the ice, snow, and graupel mass mixing ratios. For example, the two runs produce very different vertical profiles of cloud ice, which is more abundant in the WSM6 run than in the THOM run (Fig. 5c). Overall, the THOM run produces more latent heat release than the WSM6 run (Fig. 5f), energetically consistent with the overall result that the simulated TC vortex is stronger in the THOM run than the WSM6 run.

b. *Microphysical budget comparison for warm rain processes*

The differences in the latent heat release through parameterized microphysical processes between the THOM and WSM6 runs reflect the differences in the pathways to hydrometeor production (i.e., cloud and precipitation) between the schemes. In both schemes, the production of a hydrometeor represents interactions between categories of water substances (including both vapor and hydrometeors) responsible for the formation and destruction of the hydrometeor. As mentioned earlier, quantitatively different pathways are assumed in the two schemes, leading to the change of water vapor content and the formation of hydrometeors. In the development of deep convective clouds essential to TC genesis and intensification, there are diverse interactions between the various cloud hydrometeors. Furthermore, these interactions have strong feedbacks to the dynamics of clouds through modulation of buoyancy forcing via latent heat release.

Given the complexity of the interaction between the different phases of water in MP schemes and their strong feedback to cloud dynamics, it is difficult to discern the differences in parameterized microphysical processes between different MP schemes by only examining the model-simulated precipitation and hydrometeor distributions. A more physically meaningful way to compare various MP schemes is to examine the individual parameterized microphysical processes appearing in MP schemes as the sources and sinks in the prognostic equations of hydrometeors under the same meteorological forcing and feedback conditions. This approach to comparing MP schemes is a budget comparison of contributing processes for hydrometeor production and destruction. Since the THOM run produces more latent heat release than the WSM6 run in both warm and cold clouds (see the two maxima of latent heating in Fig. 5f), the microphysical budget is first compared at 4 and 5 h into the simulation when only warm-rain processes occur.

Figure 6 shows the profiles of the domain-averaged cloud water mass mixing ratio, all the microphysical contributing terms to the total tendency of cloud water mass mixing ratio referred to as the budget terms, and

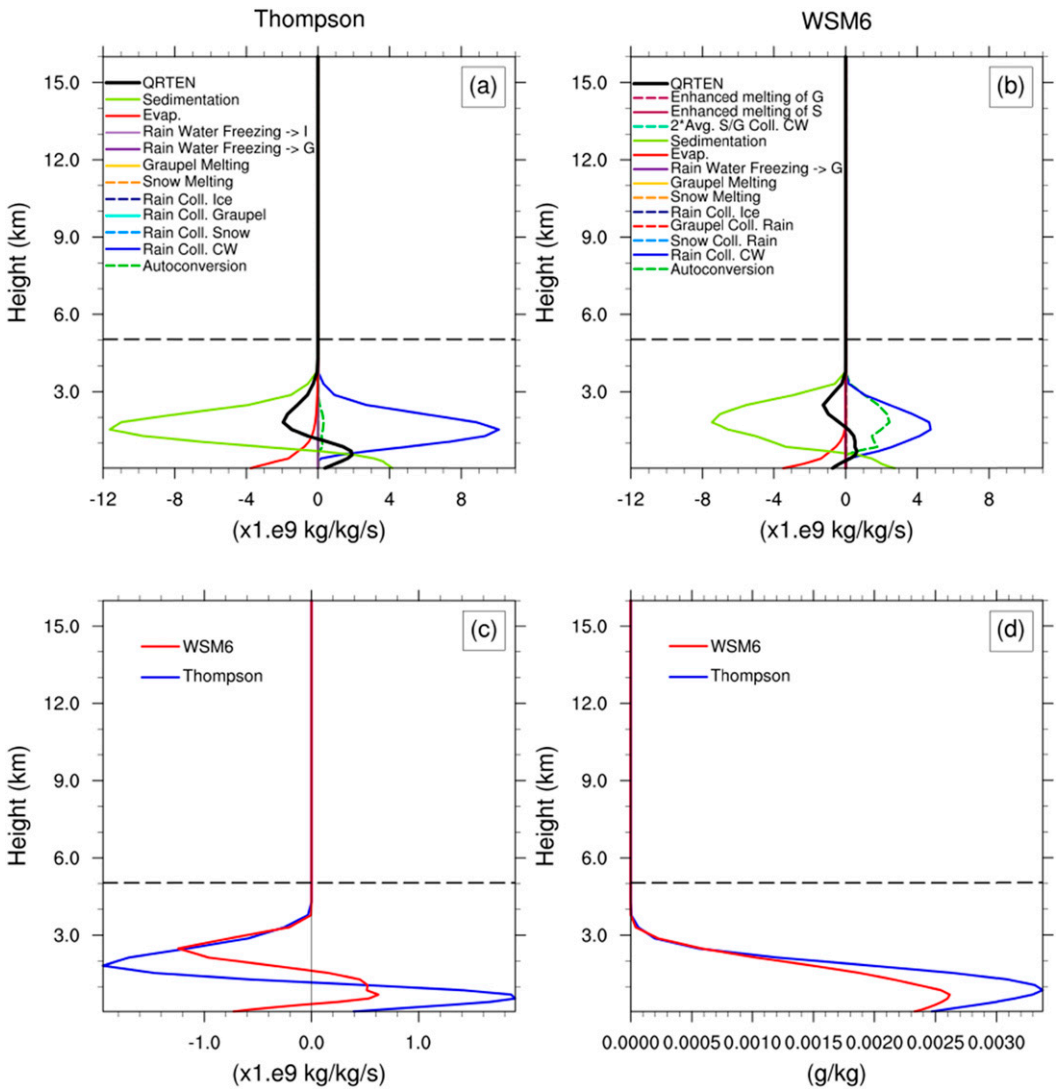

FIG. 8. The vertical profiles of the domain average of the rainwater mass mixing ratio tendency budget (scaled by 10^9) for (a) the THOM and (b) the WSM6 runs at forecast hour 5. The legends are explained in Table 3. The black dashed line is the 0°C line. The vertical profiles of the domain average of (c) the rainwater mass mixing ratio tendency (scaled by 10^9) and (d) the rainwater mass mixing ratio. In both (c) and (d), the red lines are the WSM6 run and the blue lines are the THOM run.

the sum of these terms referred to as the microphysical tendency from the THOM and WSM6 runs at hour 4 into the simulation. All the budget terms for cloud water are described in Table 2. For both runs, the tendency of cloud water mass mixing ratio is dominated by the condensation/evaporation term, and the condensation and evaporation rates for both runs are very similar at this hour. One hour later (Fig. 7), more differences in the cloud water mass mixing ratio budgets can be seen between the two runs. First, below 1 km, the THOM run produces slightly more cloud water than the WSM6 run (Fig. 7d). As shown in the budget terms (Figs. 7a and 7b), this slightly greater amount of cloud water in the THOM run is due to more condensation occurring in the THOM run than the WSM6 run. The WSM6 run has more autoconversion of cloud water to rainwater below 3 km than the THOM run, while the THOM run has a greater rate of rain collecting cloud water. Both simulations have a net sink of cloud water above 1 km, as cloud water is being converted to rainwater, albeit at different conversion rates.

The budget terms in the rainwater tendencies of the two MP schemes are described in Table 3. As shown in Figs. 8a and 8b, the sinks of cloud water are sources of

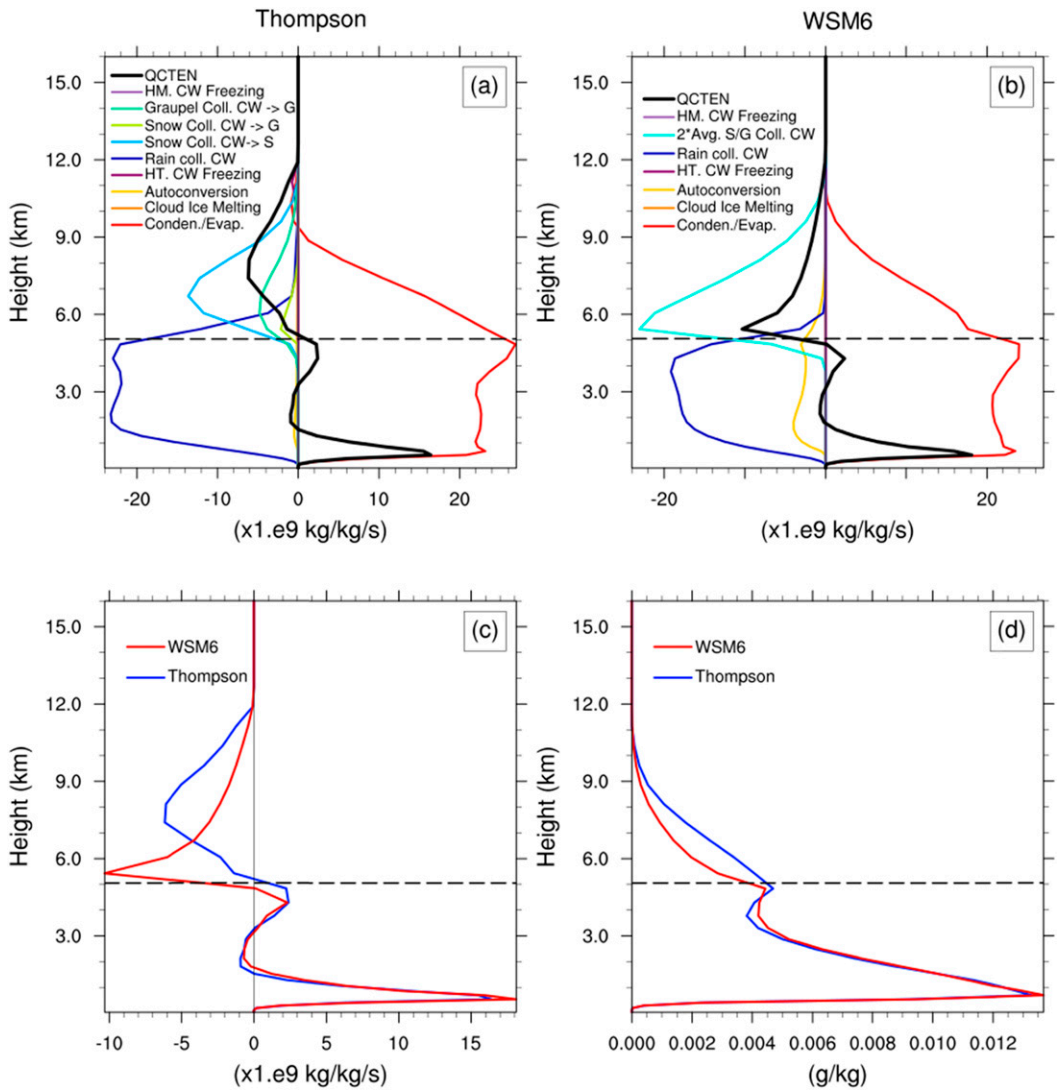

FIG. 9. The vertical profiles of the domain average of the microphysical budget of the cloud water mass mixing ratio tendency (scaled by 10^9) for (a) the THOM and (b) the WSM6 runs averaged over 1–24 h. The legends are explained in Table 2. The black dashed line is the 0°C line. The vertical profiles of the domain average of (c) the cloud water mass mixing ratio tendency (scaled by 10^9) and (d) the cloud water mass mixing ratio. In both (c) and (d), the red lines are the WSM6 run and the blue lines are the THOM run.

rainwater. The THOM run produces more rainwater than the WSM6 run below 2 km by hour 5 (Fig. 8d). The budget terms clearly show that the change in rainwater below 2 km is due largely to sedimentation from layers above. The fact that the collection of cloud water by rainwater in the THOM run is larger than the WSM6 run and more sedimentation is occurring at about 1.5 km indicates that the size of the raindrops is larger and/or fall speeds are greater in the THOM run compared to the WSM6 run. Since convective updrafts will transport some of the cloud and rainwater above the freezing level, the differences in the warm rain processes between the two runs will lead to different amounts of supercooled cloud and rainwater.

The results discussed above show that the initial production rates of cloud water are very similar, indicating no tangible numerical difference in formulations for cloud condensation, although later interactions of cloud water with other hydrometeors result in different average vertical profiles of cloud water. Initial differences in rainwater are due to the different conversion rates of cloud water to rainwater. Although the conversion of cloud to rainwater does not directly lead to latent heat release, it can contribute significantly to

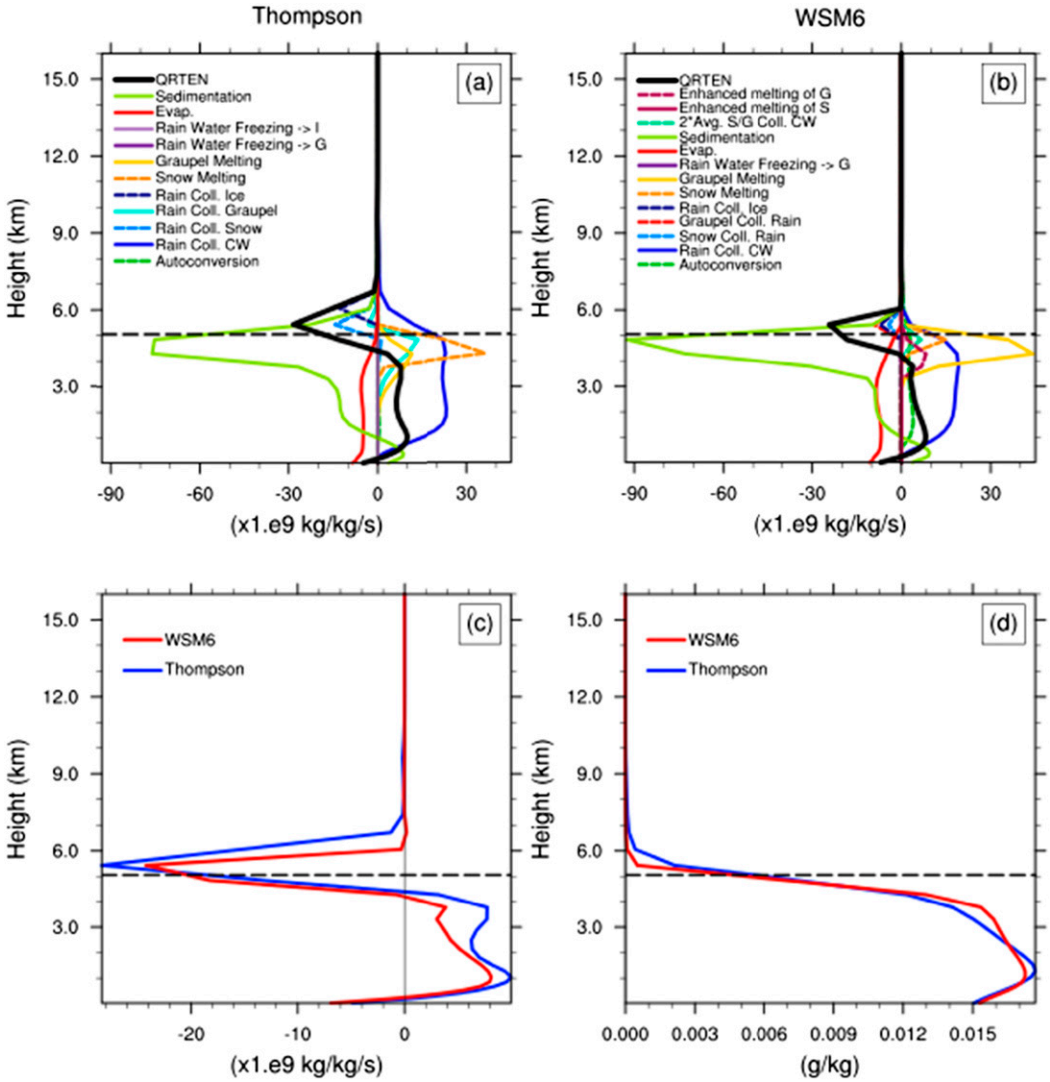

FIG. 10. The top two panels are the vertical profiles of the domain average of the microphysical budget of the rainwater mass mixing ratio tendency (scaled by 10^9) for (a) the THOM and (b) the WSM6 runs averaged from 1-24 hours. The legends are explained in Table 3. The bottom two panels are the domain average of (c) the microphysical tendencies of rainwater mass mixing ratio (scaled by 10^9) and (d) the rainwater mass mixing ratio from the two runs (in both, the red line is the WSM6 run and the blue line is the THOM run). The black dashed line is the 0°C line.

the variations in the frozen hydrometeor production and in the overall latent heat release above the freezing level. The rates of condensation after nucleation and collection growth of cloud and rainwater drops are, in principle, dependent on the size distributions of condensation nuclei and cloud drops [see, e.g., chapter 15 in Pruppacher and Klett (1997), chapter 8 in Rogers and Yau (1989), and chapter 7 in Straka (2011)]. Although the condensation rates in both the THOM and WSM6 runs are about the same, the growth rates for rainwater due to autoconversion and collection terms are not (Fig. 8). Thus, the differences in parameterized warm-rain production associated with the conversion of cloud water to rainwater reflect the basic differences of the schemes in the definition of cloud droplet and raindrop size distributions (i.e., different empirical constants used in the mass–diameter and fall speed–diameter relations shown in Table 1) and consequently in the spectrum-dependent microphysical processes, such as accretion growth of raindrops and frozen hydrometeors along with their sedimentation. The differences in the assumed size distributions of both cloud water and rainwater also can affect the net latent heating due to the fact that the evaporative cooling rate of rainwater is strongly size dependent.

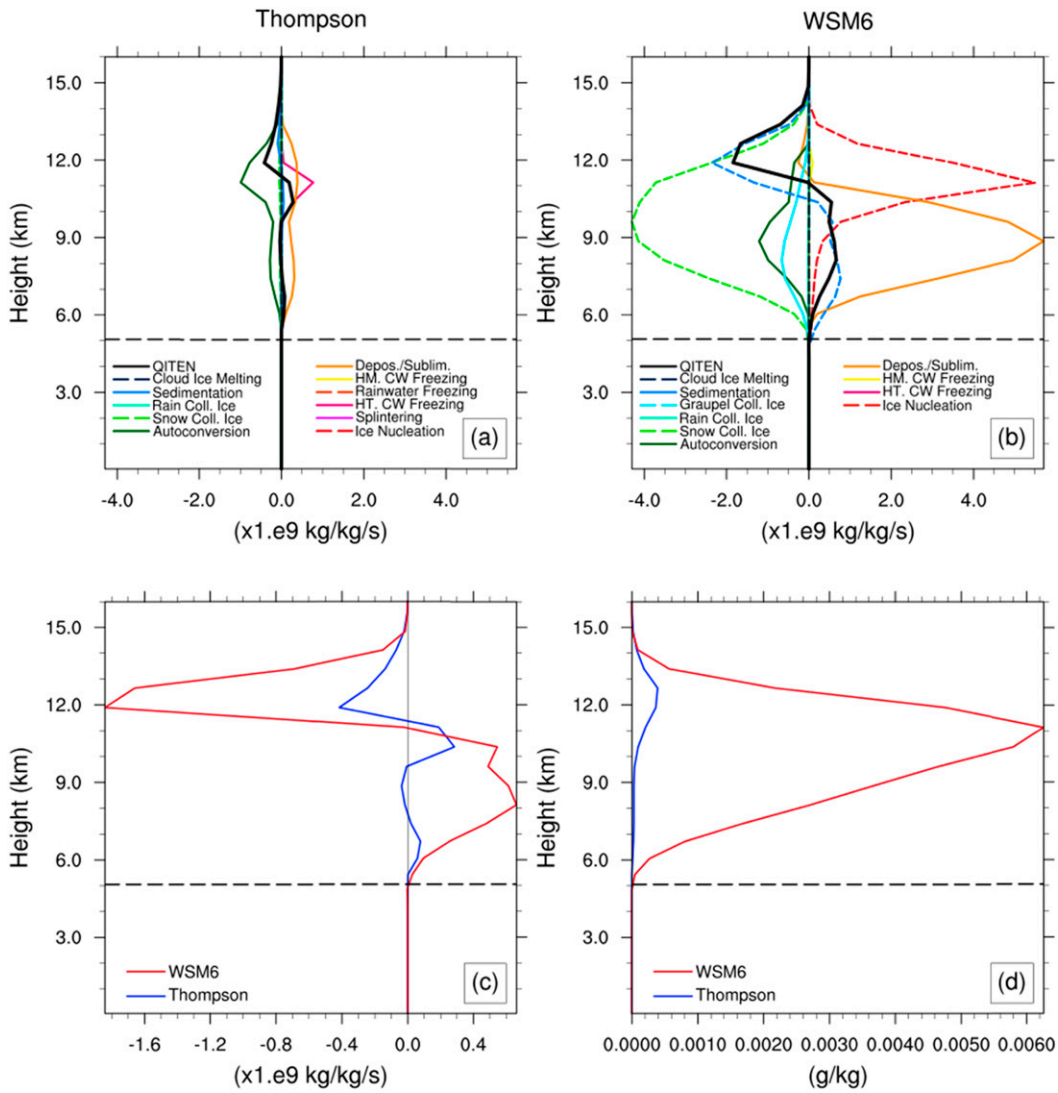

FIG. 11. Vertical profiles of the domain average of the cloud ice mass mixing ratio tendency budget (scaled by 10^9) for (a) the THOM and (b) the WSM6 runs averaged over 1–24 h. The legends are explained in Table 4. The black dashed line is the 0°C line. The domain average of (c) the cloud ice mass mixing ratio tendency (scaled by10^9) and (d) the cloud ice mass mixing ratio (in both, the red line is the WSM6 run and the blue line is the THOM run).

c. *Microphysical budget comparison for cold rain processes*

In the ensuing hours of the simulations, condensation and accretion processes that produce cloud water and rainwater continue occurring. Both cloud water and rainwater are lofted above the freezing level by updrafts to form supercooled drops at the larger end of the size distribution, which contributes to cloud glaciation and enhances the production of precipitation in cold clouds. Observations have long been supportive of this notion (see, e.g., Cober et al. 1996). Figures 9 and 10 show vertical profiles of the domain-averaged microphysical budget of the cloud water and rainwater mass mixing ratios and their tendencies from the THOM and WSM6 runs averaged from 1 to 24 h into the simulations. It is interesting to note that condensation and collection of cloud water by rainwater are significant contributors to the changes in cloud water and rainwater in the two schemes, but the magnitudes of these terms are not the same. In particular, the rates of condensation and rain collecting cloud water are greater in the THOM run than in the WSM6 run. In the THOM run, the sinks of cloud water due to collection processes involving frozen hydrometeors (snow or graupel) are parameterized by three separate budget terms, each with a maximum

TABLE 4. Terms in the cloud ice mass mixing ratio budget equation, used in the legend of Fig. 11. Actual variable names in the WRF code, where applicable, are also included in parentheses.

Legend name for THOM	Legend name for WSM6	Description
QITEN	QITEN	Cloud ice mass mixing ratio tendency
Cloud ice melting	Cloud ice melting (pimlt)	Melting of cloud ice to form cloud water
Sedimentation	Sedimentation	Sedimentation of cloud ice
	Graupel coll. ice (pgaci)	Graupel collecting cloud ice to form larger graupel
Rain coll. ice (pri_rci)	Rain coll. ice (praci)	Rain collecting cloud ice to form graupel
Snow coll. ice (prs_sci)	Snow coll. ice (psaci)	Snow collecting cloud ice to form snow
Autoconversion (prs_iau)	Autoconversion (psaut)	Autoconversion of cloud ice to snow
Depos./sublim. (pri_ide)	Depos./sublim. (pidep)	Deposition/sublimation of cloud ice
HM. CW freezing	HM. CW freezing (pihmf)	Homogeneous freezing of cloud water to cloud ice ($T < -40°C$)
Rainwater freezing (pri_rfz)		Freezing of rainwater to form cloud ice
HT. CW freezing (pri_wfz)	HT. CW freezing (pihtf)	Heterogeneous freezing of cloud water to form cloud ice ($-40° \leq T < -0°C$)
Splintering (prs_ihm)		Breakup of riming snow to form cloud ice
Ice nucleation (pri_inu)	Ice nucleation (pigen)	Cloud ice nucleation

magnitude at a different vertical level. In the WSM6 run, there is only a single term for this collection process, and the maximum magnitude occurs just above the melting level, contributing to a difference in the vertical distribution of the total cloud water tendencies. The difference in the tendency of rainwater above the freezing level shown in Fig. 10c is due to more depletion of rainwater associated with the collision of supercooled rainwater drops with precipitating frozen hydrometeors (i.e., snow and graupel) in the THOM run than the WSM6 run. The difference in the tendency of rainwater below the freezing level is due to more rainwater evaporation in the WSM6 run than the THOM run.

The processes responsible for cloud ice production between the two runs are compared in Fig. 11. The contributing terms to the total tendency are explained in Table 4. It is obvious that the WSM6 run generates significantly more ice during the first 24 h of the simulation. In the WSM6 run, the dominant production terms are nucleation and ice growth by deposition, while in the THOM run, the primary source terms are deposition and the freezing of cloud water. In both schemes, autoconversion of ice to snow is an important sink, although in the WSM6 run, collection of ice by snow and graupel has a net larger contribution. A significant difference between the two runs is that in the WSM6 run sedimentation is a significant mechanism in redistributing the cloud ice, while in the THOM run this effect is so small that most of the cloud ice is suspended in the air all of the time. This difference is due to the fact that the mean size of cloud ice is greater in the WSM6 scheme than in the THOM scheme (not shown), a result of the assumption that ice particles large than 300 μm in the THOM scheme are categorized as snow.

Figure 12 depicts differences in the processes responsible for snow production between the two runs, and the contributing terms to the total tendency of snow are described in Table 5. This figure clearly shows that the two schemes assume different pathways in snow production/destruction, as well as different pathways in graupel production. Specifically, there is more snow production above 7 km through deposition in the THOM run than in the WSM6 run. Destruction of snow through collection by rain is an important mechanism in the WSM6 run, but not in the THOM run. This is a process that leads to graupel formation and thus, contributes to the production of more graupel in the WSM6 run than the THOM run (Fig. 13d). Examining the budget terms for the graupel tendencies (Figs. 13a and 13b) confirms the different pathways in the production/destruction of graupel between the two schemes (see Table 6 for a description of all the budget terms). The magnitudes of the collection terms and sedimentation terms for graupel production are greater in the WSM6 run than in the THOM run. Furthermore, in the THOM run, the sinks of graupel below the freezing line are primarily melting and collection by rain, while there is no significant rain collecting graupel term below the freezing line as a pathway to graupel destruction in the WSM6 run.

d. Double-moment description of pathways to rainwater production

Prognostic equations of hydrometeor mass mixing ratios in all the MP schemes used in NWP models fundamentally describe the evolution of moments of the distribution functions of these hydrometeors (see, e.g., Beheng 2010). Single-moment schemes are designed to predict the evolution of the mass-equivalent moments (simply the mass mixing ratios of hydrometeors in most schemes). These schemes assume that the slope of the distribution function λ is constant, while the intercept of

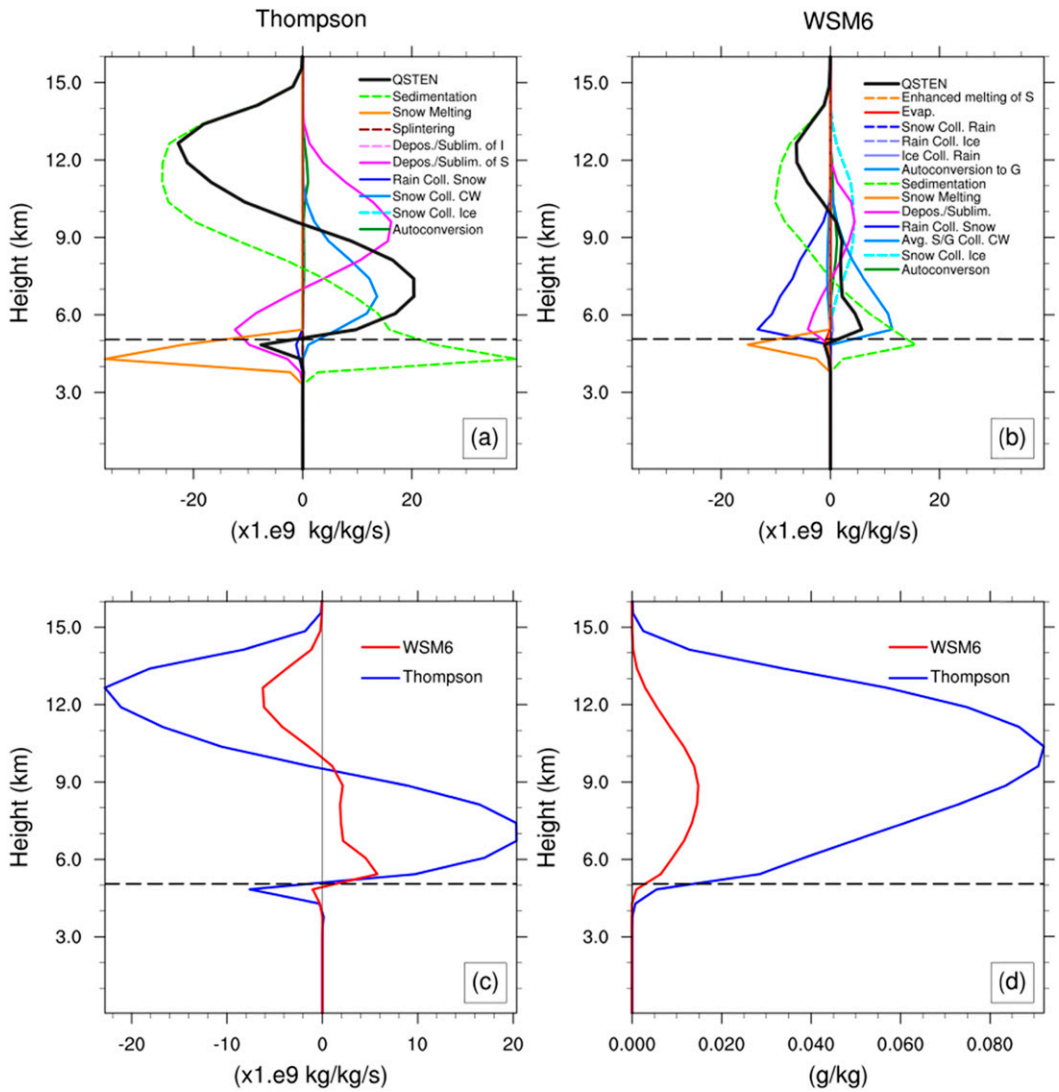

FIG. 12. Vertical profiles of the domain average of the snow mass mixing ratio tendency budget (scaled by 10^9) for (a) the THOM and (b) the WSM6 run averaged over 1–24 h. The legends are explained in Table 5. The black dashed line is the 0°C line. The domain average of (c) the snow mass mixing ratio tendency (scaled by 10^9) and (d) the snow mass mixing ratio (in both, the red line is the WSM6 run and the blue line is the THOM run).

the distribution function N_0 is proportional to the environmental state or a constant. It has become increasingly popular to expand the number of prognostic moments in MP schemes suitable for NWP models beyond the mass-equivalent moments. The advantage of the multimoment schemes, in theory, is that they predict the number mixing ratio in addition to mass mixing ratio, which allows a dynamic representation of the characteristics of the hydrometeor size distribution and enables a better representation of the processes involved in the individual pathways to hydrometeor production (see Milbrandt and Yau 2005; Cotton et al. 2010). The additional moments can also be useful for simulating the interaction of clouds with radiation, chemical constituents, etc., if these interactions are supported by the other model physics.

As mentioned in section 2, a major difference between the two MP schemes investigated in this study is that the THOM scheme includes prognostic equations for cloud ice and rainwater particle number mixing ratio. Figure 14 shows the domain-averaged vertical profiles of rainwater mass mixing ratio and the number mixing ratio of rainwater drops averaged from 1 to 24 h. The size distribution in the THOM run, as rendered by the additional prognostic equation of the number mixing ratio, is clearly shown to be different from that

TABLE 5. Terms in the snow mass mixing ratio budget equation, used in the legend of Fig. 12. Actual variable names in the WRF code, where applicable, are also included in parentheses.

Legend name for THOM	Legend name for WSM6	Description
QSTEN	QSTEN	Snow mass mixing ratio tendency
Sedimentation	Sedimentation	Sedimentation of snow
Snow melting (prr_sml)	Snow melting (psmlt)	Snow melting to form rain
Splintering (prs_ihm)		Breakup of riming snow to form cloud ice
Depos./sublim. of I (prs_ide and prs_sde)	Depos./sublim. (psdep)	Deposition growth of large cloud ice to form snow
Depos./sublim. of S		Deposition/sublimation of existing snow
Rain coll. snow (prs_rcs)	Rain coll. snow (pracs)	Rain collecting snow to form snow ($T < 0°C$) or rain ($T \geq 0°C$) in THOM, but to form graupel in WSM6
Snow coll. CW (prs_scw)	Avg. S/G coll. CW (paacw)	Snow collecting cloud water to form snow and graupel if $T < 0°C$, but to form rain if $T \geq 0°C$
Snow coll. ice (prs_sci)	Snow coll. ice (psaci)	Snow collecting cloud ice to form snow of larger sizes
Autoconversion (prs_iau)	Autoconversion (psaut)	Autoconversion of cloud ice to snow
	Enhanced melting of S (pseml)	Enhanced melting of snow by accretion of rainwater
	Evap (psevp)	Evaporation of melting snow ($T \geq 0°C$)
	Snow coll. rain (psacr)	Snow collecting rain to form snow/graupel ($T < 0°C$) or rain ($T \geq 0°C$)
	Rain coll. ice (praci)	Rain collecting ice to form snow or graupel ($T < 0°C$)
	Ice coll. rain (piacr)	Cloud ice collecting rain to form either snow or graupel ($T < 0°C$)
	Autoconversion to G (pgaut)	Autoconversion (aggregation) of snow to form graupel ($T < 0°C$)

diagnosed in the WSM6 run. If the mass of rainwater is quite similar, but the number of drops is larger (smaller), it means that the droplet size must be smaller (larger). In Fig. 14, the size of the raindrops near the surface is significantly greater in the THOM run, where the number mixing ratio is about $80\,kg^{-1}$ compared to the WSM6 run, which is more than $170\,kg^{-1}$, for a similar mass of rain ($\sim 0.015\,g\,kg^{-1}$). This is equivalent to about 1.9×10^{-4} grams per particle in the THOM run and 8.8×10^{-5} grams per particle in the WSM6 run. Conversely, above the freezing level, the THOM run has higher number mixing ratios and therefore smaller droplets. In the warm clouds between 3 km and the freezing level, the size of raindrops is also greater in the THOM run than in the WSM6 run. The microphysical processes responsible for the change of rainwater number mixing ratio in single-moment schemes, such as the WSM6 scheme, are the same as those responsible for the mass mixing ratio change since the number mixing ratio is determined by the mass mixing ratio. In double-moment schemes, however, there are processes that are responsible for changing the rainwater number mixing ratio, but do not change the mass mixing ratio, such as self-collection and breakup of rainwater drops.

Figure 15 depicts the microphysical budget for the tendency of rainwater number mixing ratio from the THOM run for the time period 1–24 h. The budget terms are explained in Table 7. As shown in Figs. 10a and 10b, the prominent processes that contribute to the change of rainwater mass mixing ratio are evaporation, sedimentation, collection of other species by raindrops, melting of precipitating frozen hydrometeors, and autoconversion (WSM6 only). It is shown in Fig. 15 that the number mixing ratio budget in the THOM run includes all the prominent processes responsible for the change of rainwater mass mixing ratio, with two notable exceptions. First, the collection of cloud water by rain is a process that is important in the mass tendency but does not change the number mixing ratio of rainwater. Second, there is an additional process that only the double-moment scheme can account for: self-collection of rainwater drops ("Rain coll. Rain" in Fig. 15). The inclusion of the self-collection process enables the THOM scheme to mimic an important pathway to the size growth of rainwater drops. The contribution to the rate of change of rainwater number mixing ratio by sedimentation is also different than that diagnosed from the mixing ratio budget in the WSM6 run. This is because in the THOM scheme the fall speed for the sedimentation of number mixing ratio is number weighted, while in the WSM6 scheme the fall speed is mass weighted. It is worth pointing out that theoretically it is advantageous to apply different sedimentation rates to number mixing ratio and mass mixing ratio in the THOM scheme. Unlike in the budget for the rate of change of the rainwater mass mixing ratio in the WSM6 run where the autoconversion term is counterbalanced only by the evaporation term above the surface (see Fig. 10b), in the

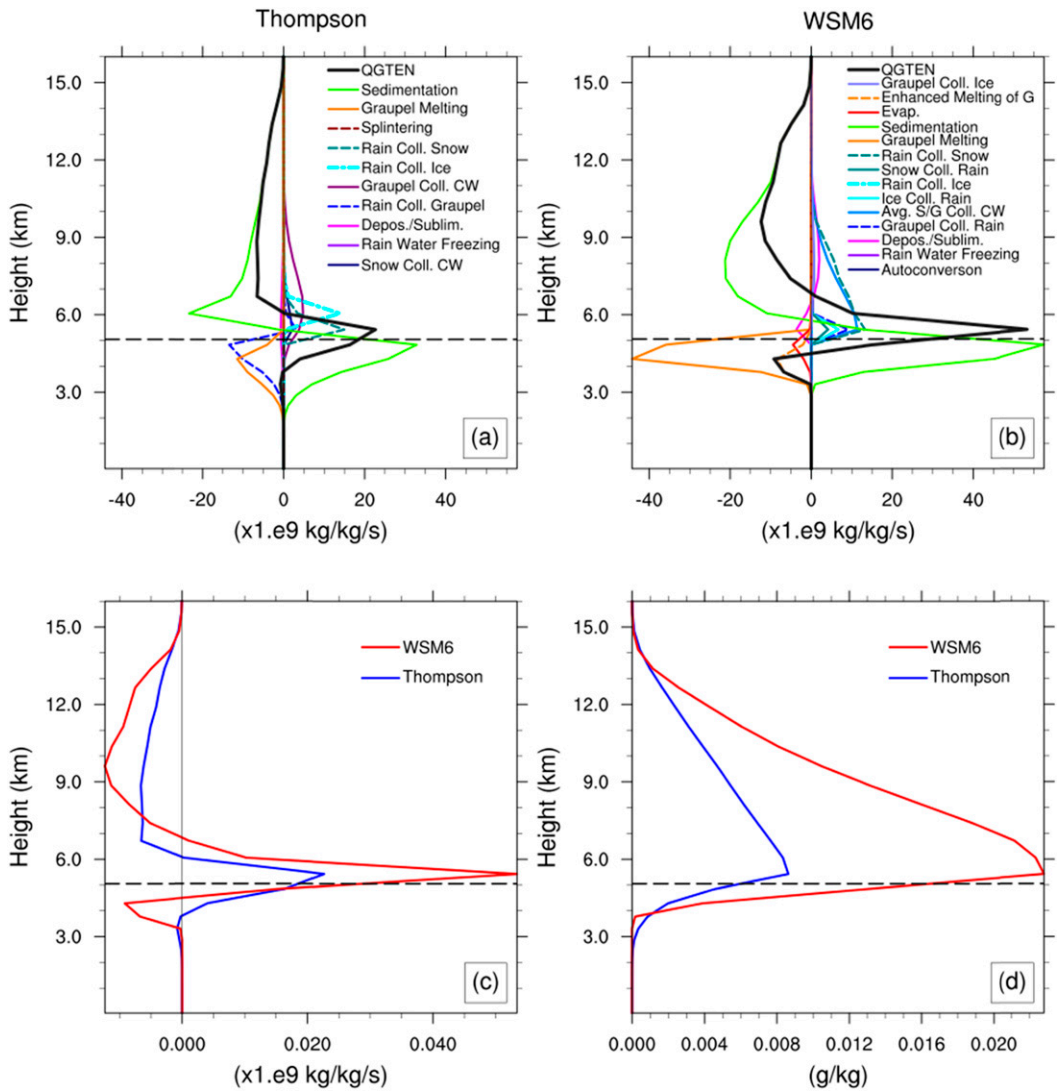

FIG. 13. Vertical profiles of the domain average of the graupel mass mixing ratio tendency budget (scaled by 10^9) for (a) the THOM and (b) the WSM6 runs averaged over 1–24 h. The legends are explained in Table 6. The black dashed line is the 0°C line. The domain average of (c) the graupel mass mixing ratio tendency (scaled by 10^9) and (d) the graupel mass mixing ratio (in both, the red line is the WSM6 run and the blue line is the THOM run).

THOM run the autoconversion term in the rainwater number mixing ratio budget is counteracted by both evaporation and self-collection.

The collection of cloud water and small rainwater drops by large rainwater drops in warm clouds is an important growth mechanism and contributes effectively to the amount of rainfall reaching the ground (Kessler 1969; Beard and Ochs 1984). Generally speaking, double-moment schemes are capable of describing the size sorting of precipitating hydrometeors (Milbrandt and McTaggart-Cowan 2010) and the self-collection and collisional breakup of rainwater drops (Beheng 2010; Van Weverberg et al. 2012; Morrison et al. 2012) that single-moment schemes cannot. It is important to note that there are great variations in the quantitative formulations of both self-collection and collisional breakup terms, and the rainwater production in double-moment schemes is sensitive to variation in these two terms (Straka 2011). Instead of explicitly including self-collection and collisional breakup terms, the THOM scheme only contains the process formulation for self-collection of rainwater drops and the effect of rainwater drop breakup is parameterized as an adjustment to the collection efficiency (Verlinde and Cotton 1993).

It should be pointed out that the differences in the number mixing ratio profiles shown in Fig. 14 are not

TABLE 6. Terms in the graupel mass mixing ratio budget equation, used in the legend of Fig. 13. Actual variable names in the WRF code, where applicable, are also included in parentheses.

Legend name for THOM	Legend name for WSM6	Description
QGTEN	QGTEN	Graupel mass mixing ratio tendency
Sedimentation	Sedimentation	Sedimentation of graupel
Graupel melting (prr_gml)	Graupel melting (pgmlt)	Melting of graupel
Splintering (prg_ihm)		Breakup of graupel to form cloud ice
Rain coll. snow (prg_rcs)	Rain coll. snow (pracs)	Rain collecting snow to form graupel
	Snow coll. rain (psacr)	Snow collecting rain to form snow or graupel for $T < 0°C$; for $T \geq 0°C$, to form rain as part of enhanced melting of snow
Rain coll. ice (prg_rci)	Rain coll. ice (praci)	Rain collecting ice to form graupel in THOM, but to form both snow and graupel in WSM6
	Ice coll. rain (piacr)	Cloud ice collecting rain to form either snow or graupel ($T < 0°C$)
Graupel coll. CW (prg_gcw)	Avg. S/G coll. CW (paacw)	Graupel and snow collecting cloud water to form graupel
Snow coll. CW (prg_scw)		(WSM6: for $T < 0°C$, also forms snow, for $T \geq 0°C$, produces rain)
Rain coll. graupel (prg_rcg)		Rain collecting graupel to form graupel of larger size ($T < 0°C$) or rain ($T \geq 0°C$)
Depos./sublim. (prg_gde)	Depos./sublim. (pgdep)	Deposition and sublimation of existing graupel
Rain water freezing (prg_rfz)	Rain water freezing (pgfrz)	Freezing of rainwater to form graupel
	Graupel coll. ice (pgaci)	Graupel collecting ice to form graupel ($T < 0°C$)
	Enhanced melting of G (pgeml)	Enhanced melting of graupel ($T \geq 0°C$)
	Evap. (pgevp)	Evaporation of melting graupel ($T \geq 0°C$)
	Autoconversion (pgaut)	Autoconversion of snow to graupel
	Graupel coll. rain (pgacr)	Graupel collecting rain to form graupel if $T < 0$; if $T \geq 0$ to form rain as a part of enhanced melting of graupel by accretion of water

only caused by the differences between the single- and double-moment formulations, but also by the differences in the formulations of the budget terms. The latter differences are associated with those in the assumed size distributions of precipitating hydrometeors between the two schemes (e.g., different empirical constants used in the mass–diameter and fall speed–diameter relations). Although the double-moment formulation has an advantage in describing a change in number mixing ratio due to large raindrops collecting small raindrops and the effect of subgrid-scale variability in evaporation below cloud base as shown by Seifert (2008), there have been neither sufficient observations nor sound theories to ascertain the accuracy of the individual budget terms contributing to the number mixing ratio changes of rainwater as shown in Fig. 15. Further, various cloud microphysical processes act as negative (i.e., counteracting) feedbacks as represented by positive and negative terms in the microphysical tendency equation of a hydrometeor and, therefore, they are highly nonlinear due to numerous interactions between these processes. All these make it difficult to discern in studies like this one which of the two schemes is more theoretically and practically advantageous to be used for TC prediction models. Thus, given the differences in the hydrometeor size distributions assumed in the two schemes, the results shown in Figs. 14 and 15 highlight the possibility that the theoretical advantage of the double-moment formulation over the single-moment formulation can be overshadowed by the uncertainties in the spectrum-dependent formulations of the individual terms contributing to the total local tendency of hydrometeor number mixing ratio.

e. Double-moment description of pathways to cloud ice production

Figure 16 shows the domain-averaged vertical profiles of cloud ice mass mixing ratio and the number mixing ratio of cloud ice averaged from 1 to 24 h. Noting that the scales differ in the two plots, it is easily seen that the THOM run produces much less cloud ice than the WSM6 run. Budget comparison for the cloud ice mass mixing ratio tendency (Fig. 11) indicates that this results from the difference in the size definition of cloud ice between the two schemes. In fact, cloud ice particles with diameters greater than 300 μm in the THOM scheme are categorized as snow through the autoconversion term, while frozen particles with diameters as large as 500 μm are categorized as ice in WSM6. Consistently, the sedimentation contribution to the cloud ice tendency is much smaller in the THOM run than the WSM6 run, resulting in the elevation of the

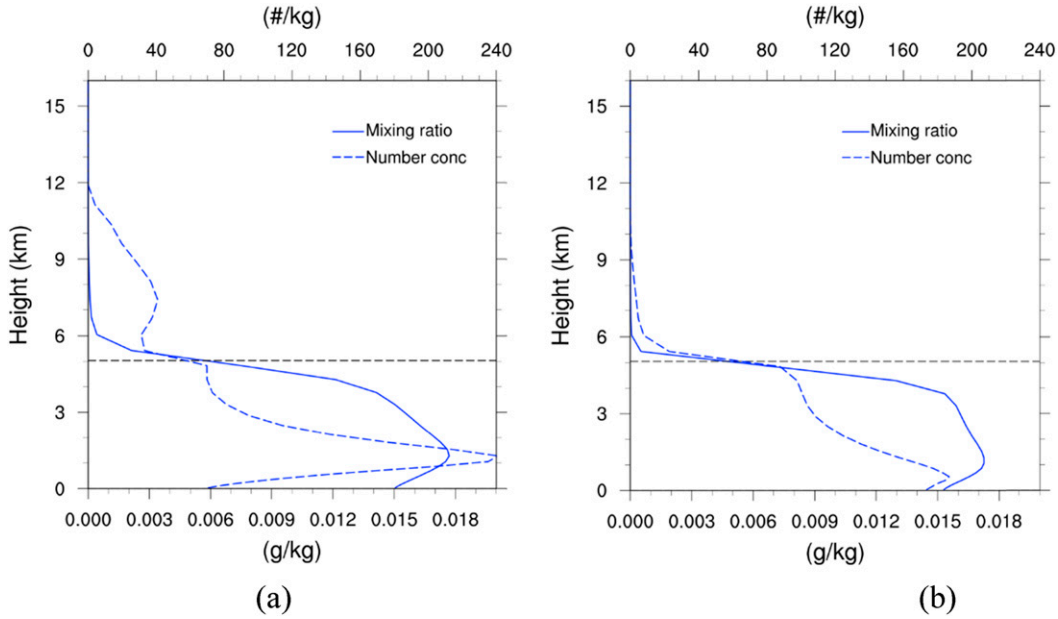

FIG. 14. Domain-averaged vertical profiles of rainwater mass mixing ratio (solid line, g kg^{-1}) and number mixing ratio (dashed line, kg^{-1}) averaged over 1–24 h for (a) the THOM run and (b) the WSM6 run. The bottom axis is for the mass mixing ratio and the top axis is for number mixing ratio. The black dashed line is the 0°C line.

maximum of cloud ice in the THOM run being higher than that in the WSM6 run as seen in Fig. 16. The microphysical budget for the tendency of cloud ice number mixing ratio from the THOM run is shown in Fig. 17 and all the budget terms are described in Table 8. In the THOM scheme, adjustment terms are applied to the computed number mixing ratios of cloud ice as a constraint to ensure that the cloud ice particles are within a prescribed size range. It is shown in Fig. 17 that the magnitude of these adjustment terms is large, approximately offsetting the terms parameterizing the freezing of water droplets and instantaneous freezing of cloud water. Similar to the processes responsible for the change of rainwater and cloud ice mass mixing ratios, the processes governing the change of number mixing ratio of rainwater and cloud ice are, in principle, dependent on the size distributions of condensation nuclei and cloud drops. The magnitudes of the budget terms associated with these processes are so great and associated with the moment-specific sedimentation terms that they overshadow the differences due to the single- versus double-moment formulations.

f. Effect of microphysical processes on net latent heating

No matter how complicated an MP scheme is in an NWP model, the end effect of the scheme on the dynamics of the model is due to the latent heating associated with the phase changes of water substance in the production of cloud and precipitation. To summarize the differences in the effect on the model dynamics associated with the differences in the microphysical terms between the two schemes, Fig. 18 shows the 1–24-h average vertical profiles of domain-averaged budget terms

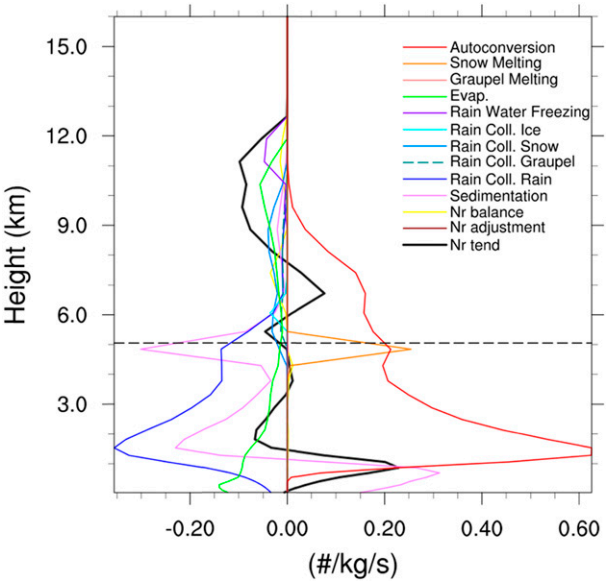

FIG. 15. The domain-averaged vertical profiles of the rainwater number mixing ratio budget averaged over hours 1–24 for the THOM run. The legends are explained in Table 7. The black dashed line is the 0°C line.

TABLE 7. Terms in the budget equation of rainwater number mixing ratio in the Thompson scheme, used in the legend of Fig. 15. Actual variable names in the WRF code, where applicable, are also included in parentheses.

Legend name	Description
Nr Tend	Rainwater number mixing ratio tendency
Autoconversion (pnr_wau)	Autoconversion of cloud water to form rainwater
Snow melting (pnr_sml)	Snow melting to form rainwater
Graupel melting (pnr_gml)	Graupel melting to form rainwater
Evap. (pnr_rev)	Evaporation of rainwater
Rain water freezing (pnr_rfz)	Freezing of rainwater to form cloud ice
Rain coll. ice (pnr_rci)	Rain collecting ice to form graupel at $T < 0°C$
Rain coll. snow (pnr_rcs)	Rain collecting snow to form snow ($T < 0°C$) or rain ($T \geq 0°C$)
Rain coll. graupel (pnr_rcg)	Rain collecting graupel to form larger graupel ($T < 0°C$) or rainwater ($T \geq 0°C$)
Rain coll. rain (pnr_rcr)	Rain collecting rain (self-collection) to form larger rain drops when the mean drop diameter is smaller than 600 μm, and drop breakup takes effect when the mean drop diameter is greater than 600 μm (quick breakup takes place when the mean drop diameter exceeds 900 μm)
Sedimentation	Sedimentation of rain drops (gravitational sorting)
Nr balance[a]	Numerical adjustment to constrain raindrops to be within the assumed size range
Nr adjustment[a]	Numerical adjustment to constrain raindrops to be within the assumed size range

[a] Both the balance and adjustment terms are numerical constraints to ensure that the corresponding hydrometeor particles remain within the assumed range of size. While the former constraint is applied right after all the microphysical terms except for sedimentation and evaporation are computed, the latter is applied after the sedimentation and evaporation are computed.

in the temperature tendency due to microphysical processes for the two experiments. All the budget terms are described in Table 9. The net tendencies resulting from these budget terms correspond to the latent heating profiles associated with the microphysics parameterizations shown in Fig. 5f. Both the THOM and WSM6 runs have the same discernable large positive terms: condensation formation of cloud water, deposition growth of precipitating frozen hydrometeors (i.e., snow and graupel), and collection terms leading to riming of cloud and rainwater on precipitating frozen hydrometeors. However, the term associated with the formation of cloud ice through ice nucleation has a significant magnitude in the WSM6 run, but in the

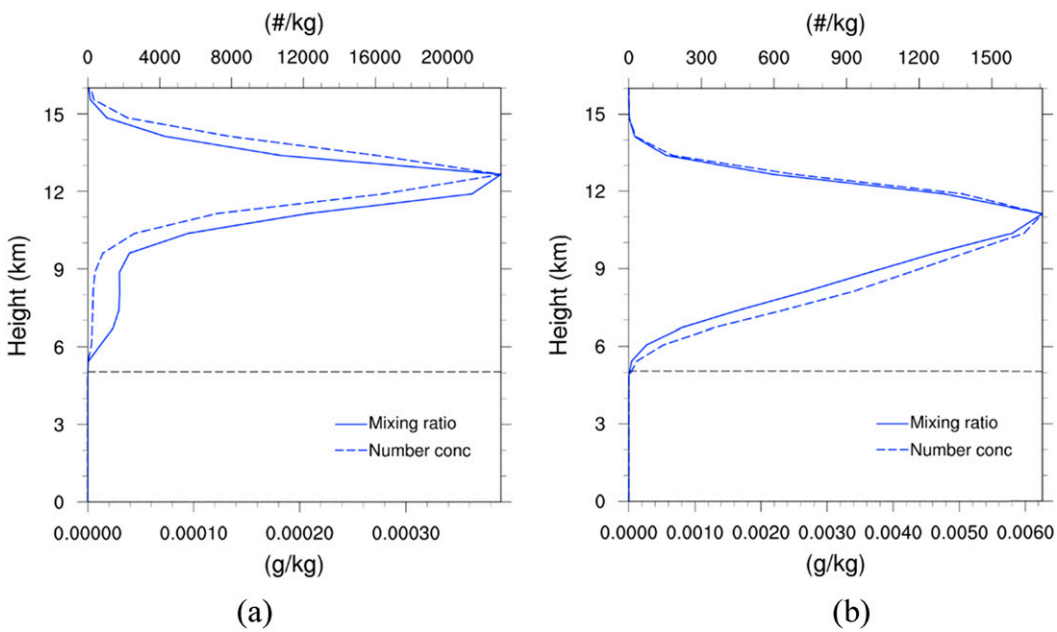

FIG. 16. Domain-averaged vertical profiles of cloud ice mass mixing ratio (solid line, g kg^{-1}) and number mixing ratio (dashed line, kg^{-1}) averaged over 1–24 h for (a) the THOM run and (b) the WSM6 run. The bottom axis is for the mass mixing ratio and the top axis is for number mixing ratio. Note the difference in scale between (a) and (b). The black dashed line is the 0°C line.

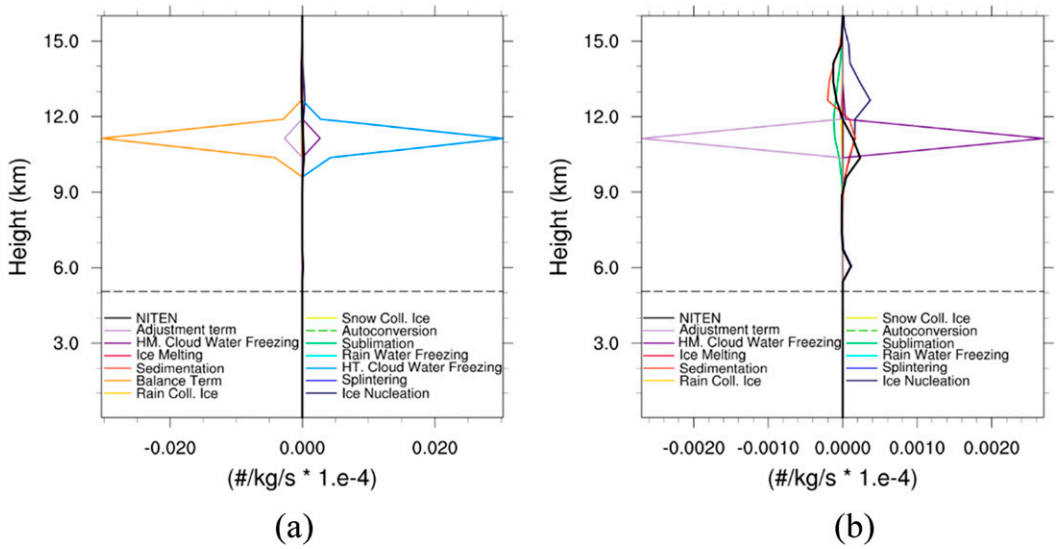

FIG. 17. (a),(b) The domain-averaged vertical profiles of the cloud ice number mixing ratio budget averaged over hours 1–24. The black lines are the cloud ice number mixing ratio tendency ($kg^{-1}\,s^{-1}$) . Panel (a) includes all the terms, while panel (b) shows all terms except the two largest terms: freezing of water droplets (blue lines) and the balance term (orange lines). All terms are scaled by 10^{-4}. The legends are explained in Table 8. The black dashed line is the 0°C line.

THOM run, it is so small that it is not discernable in Fig. 18. Both runs also have the same discernable negative terms: raindrop evaporation, sublimation of precipitating frozen hydrometeors, and melting of precipitating frozen hydrometeors. There are, however, other terms that are unique to each scheme. The THOM run has a negative term associated with the melting of precipitating frozen hydrometeors below the freezing level that does not exist in the WSM6 run (the term labeled "Coll, T>0: R+SGI=R"). Additionally, right below the freezing level, the WSM6 run has a term associated with evaporation of melting precipitating frozen hydrometeors that is not in the THOM run (the term labeled "Evap mltg SG"), while the THOM run has a term to account for sublimation of snow and graupel that is not in the WSM6 run (the term labeled "Dep/Subl T>0"). It is uncertain whether the evaporation of melting snow and graupel is a more accurate assumption of what happens in nature right below the freezing level than the sublimation of frozen snow and graupel. All these contribute to the differences in the net latent heat release between the two runs as shown

TABLE 8. Terms in the budget equation of cloud ice number mixing ratio in the Thompson scheme, used in the legend of Fig. 17. Actual variable names in the WRF code, where applicable, are also included in parentheses.

Legend name	Description
NITEN	Cloud ice number mixing ratio tendency
Balance term[a]	Numerical adjustment to constrain cloud ice particles to be within the assumed size range
Adjustment term[a]	Numerical adjustment to constrain cloud ice to be within the assumed size range
HM. cloud water freezing	Homogeneous freezing of cloud water to cloud ice ($T < -40$°C)
HT. cloud water freezing (pni_wfz)	Heterogeneous freezing of rain and/or cloud water to form cloud ice ($-40° \leq T < -0$°C)
Rain water freezing (pni_rfz)	Freezing of rainwater to form cloud ice
Autoconversion (pni_iau)	Autoconversion of cloud ice to snow
Ice nucleation (pni_inu)	Cloud ice nucleation
Snow coll. ice (pni_sci)	Snow collecting cloud ice to form snow of larger size
Rain coll. ice (pni_rci)	Rain collecting cloud ice to form graupel of larger size
Splintering (pni_ihm)	Breakup of riming graupel to form cloud ice
Sublimation (pni_ide)	Sublimation of cloud ice
Ice melting	Melting of cloud ice
Sedimentation	Sedimentation of cloud ice (gravitational sorting)

[a] See the note at the bottom of Table 7.

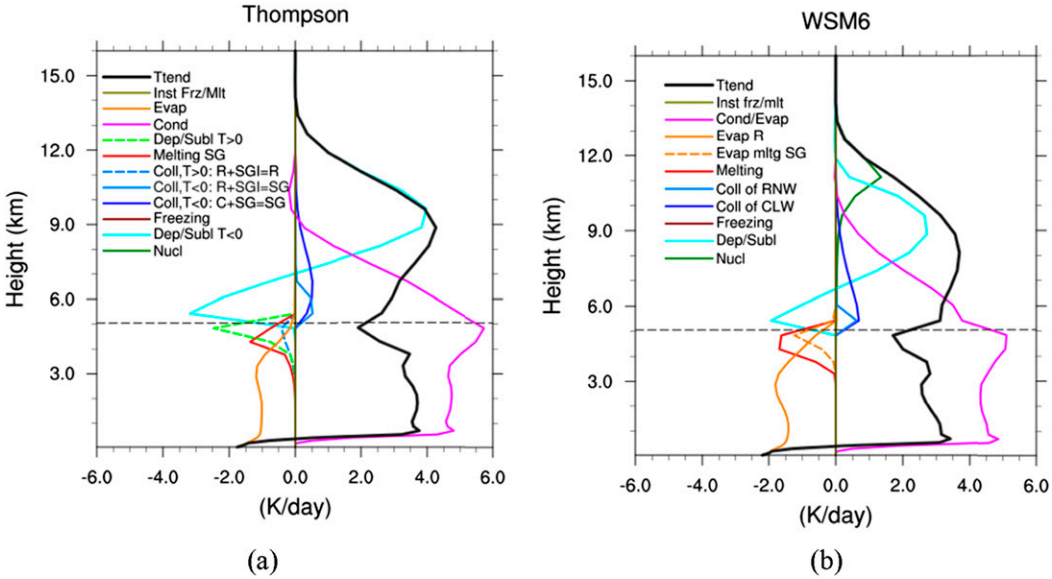

FIG. 18. Time averaged (1-24 h) vertical profiles of domain-averaged budget terms in the temperature tendency from the (a) THOM run and (b) WSM6 run corresponding to the latent heating profiles associated with microphysics. The legends are explained in Table 9. The black dashed line is the 0°C line.

in Fig. 5f, resulting in the difference in the simulated TC intensification.

4. Summary and conclusions

This study is intended to address the two questions raised in the introduction about the major microphysical processes affecting the simulated initial rapid intensification and the fundamental differences of two microphysics parameterization schemes available in the WRF Model. To this end, we first show the differences in the simulated intensification and structural evolution of an idealized TC between the WSM6 and THOM schemes in the WRF Model. These differences simply reflect the

TABLE 9. Terms in the temperature budget equation, used in the legend of Fig. 18. Actual variable names in the WRF code are, where applicable, also included in parentheses. Terms have been grouped by process.

Legend name for THOM	Legend name for WSM6	Description
Ttend	Ttend	Temperature tendency for microphysical processes
Inst frz/mlt	Inst frz/mlt (pimlt, pihmf)	Homogeneous freezing, $T < T_{crit}$ Instantaneous melting $T \geq 0°C$
Evap (prv_rev)	Evap R (prevp)	Evaporation of rainwater
Cond (prw_vcd)	Cond/evap (pcond)	Condensation and evaporation of cloud water
	Evap mltg SG (psevp, pgevp)	Evaporation of melting snow and graupel
Dep/subl T > 0 (prs_sde, prg_gde)		Deposition/sublimation when $T \geq 0°C$
Melting SG (prr_sml, prr_gml)	Melting (psmlt, pgmlt, pseml, pgeml)	Melting, including enhancement by collisions with liquid
Coll, T > 0: R+SGI=R (prr_rcg, prr_rcs)		Rain collecting snow, graupel, and/or cloud ice to form rain
Coll, T < 0: R+SGI=SG (prg_rcs, prs_rcs, prr_rci, prg_rcg)	Coll of RNW (piacr, pgacr, psacr)	Rain collecting snow, graupel, and/or cloud ice to form snow and/or graupel
Coll, T < 0: C+SG=SG (prs_scw, prg_scw, prg_gcw)	Coll of CLW (paacw*2)	Snow and/or graupel collecting cloud water to form snow and/or graupel
Freezing (pri_wfz, pri_rfz, prg_rfz)	Freezing (pihtf, pgfrz)	Freezing of water drops $T_{crit} < T \leq 0°C$
Dep/subl T < 0 (pri_ide, prs_ide, prs_sde, prg_gde)	Dep/subl (psdep, pgdep, pidep)	Deposition/sublimation when $T < 0°C$
Nucl (pri_inu)	Nucl (pigen)	Ice nucleation

dynamical dependence of the simulated TC development on variations in the diabatic forcing associated with different microphysics parameterization schemes. We then compare the hydrometeor distribution and latent heating profiles from the two schemes, showing that quantitative differences in the assumed pathways to the production of hydrometeors significantly contribute to the differences in the net latent heat release between the two schemes. We further diagnose the source and sink terms of all the hydrometeor budgets.

In summary, the results from the study show the following:

- There are no significant numerical differences in the formulations of cloud water production through condensation between the WSM6 and THOM schemes in this idealized case study.
- There are noticeable differences in the cloud-to-rain conversion due to different size distribution assumptions in the parameterizations of autoconversion, collection, and sedimentation processes.
- Pathways to frozen hydrometeor production in the two schemes are significantly different mainly because of the differences in the assumed size distributions in the calculation of ice nucleation, deposition and collection growth, and hydrometeor sedimentation.
- The above differences lead to different vertical distributions of net latent heat release, resulting in different intensification and structural evolution of the simulated TC and different dynamical feedback to vertical distributions of hydrometeors.

It is demonstrated in this study that hydrometeor budget analysis is an effective tool for MP scheme comparison and evaluation studies, allowing for a better understanding of actual assumed pathways to cloud and precipitation production in these schemes. The budget analyses clearly show that the total local change of a hydrometeor due to parameterized microphysical processes is made of positive and negative terms that interplay with each other nonlinearly and act as negative feedbacks. The results from the budget analyses highlight the possibility that the differences in the microphysical processes involving the assumed hydrometeor size distributions between the WSM6 and THOM schemes may overshadow the differences between the single- and double-moment formulations. They suggest that the uncertainties in MP parameterizations associated with hydrometeor size distributions and frozen hydrometeor partitions in individual budget terms do not diminish as the parameterizations become more complex and involve multiple moments as prognostic variables. Nevertheless, the budget analysis will be useful for evaluating MP schemes in TC prediction models as we continue the effort to address the general question of what is the proper complexity in cloud microphysics parameterizations required for accurately simulating the net effects of the clouds in TCs at a given resolution.

Acknowledgments. This work is supported by the Hurricane Forecasting Improvement Project (HFIP) of NOAA. The authors thank the three anonymous reviewers and Hugh Morrison for their insightful comments and suggestions. The authors also acknowledge the use of the NCAR Command Language (NCL) in the analysis of the WRF Model output and the preparation of figures.

REFERENCES

Bao, J. W., S. G. Gopalakrishnan, S. A. Michelson, F. D. Marks, and M. T. Montgomery, 2012: Impact of physics representations in the HWRFX on simulated hurricane structure and pressure–wind relationships. *Mon. Wea. Rev.*, **140**, 3278–3299, doi:10.1175/MWR-D-11-00332.1.

Beard, K. V., and H. T. Ochs, 1984: Collection and coalescence efficiencies for accretion. *J. Geophys. Res.*, **89**, 7165–7169, doi:10.1029/JD089iD05p07165.

Beheng, K. D., 2010: The evolution of raindrop spectra: A review of microphysical essentials. *Rainfall: State of the Science*, F. Y. Testik and M. Gebremichael, Eds., Amer. Geophys. Union, 29–48, doi:10.1029/2010GM000957.

Cober, S. G., A. Tremblay, and G. A. Isaac, 1996: Comparisons of SSM/I liquid water paths with aircraft measurements. *J. Appl. Meteor.*, **35**, 503–519, doi:10.1175/1520-0450(1996)035<0503:COSLWP>2.0.CO;2.

Cotton, W. R., G. Bryan, and S. C. van den Heever, 2010: *Storm and Cloud Dynamics*. International Geophysics, Vol. 99, Academic Press, 820 pp.

Davidson, N. E., and Coauthors, 2014: ACCESS-TC: Vortex specification, 4DVAR initialization, verification, and structure diagnostics. *Mon. Wea. Rev.*, **142**, 1265–1289, doi:10.1175/MWR-D-13-00062.1.

Dudhia, J., 1989: Numerical study of convection observed during the winter monsoon experiment using a mesoscale two-dimensional model. *J. Atmos. Sci.*, **46**, 3077–3107, doi:10.1175/1520-0469(1989)046<3077:NSOCOD>2.0.CO;2.

Ferrier, B. S., 1994: A double-moment multiple-phase four-class bulk ice scheme. Part I: Description. *J. Atmos. Sci.*, **51**, 249–280, doi:10.1175/1520-0469(1994)051<0249:ADMMPF>2.0.CO;2.

Field, P. R., R. J. Hogan, P. R. A. Brown, A. J. Illingworth, T. W. Choularton, and R. J. Cotton, 2005: Parametrization of ice-particle size distributions for mid-latitude stratiform cloud. *Quart. J. Roy. Meteor. Soc.*, **131**, 1997–2017, doi:10.1256/qj.04.134.

Gallus, W. A., Jr., and M. Pfeifer, 2008: Intercomparison of simulations using 5 WRF microphysical schemes with dual-polarization data for a German squall line. *Adv. Geosci.*, **16**, 109–116, doi:10.5194/adgeo-16-109-2008.

Gray, W. M., E. Ruprecht, and R. Phelps, 1975: Relative humidity in tropical weather systems. *Mon. Wea. Rev.*, **103**, 685–690, doi:10.1175/1520-0493(1975)103<0685:RHITWS>2.0.CO;2.

Hong, S.-Y., and J.-O. J. Lim, 2006: The WRF single-moment 6-class microphysics scheme (WSM6). *J. Korean Meteor. Soc.*, **42**, 129–151.

Houze, R. A., 2010: Clouds in tropical cyclones. *Mon. Wea. Rev.*, **138**, 293–344, doi:10.1175/2009MWR2989.1.

——, P. V. Hobbs, P. H. Herzegh, and D. B. Parsons, 1979: Size distributions of precipitation particles in frontal clouds. *J. Atmos. Sci.*, **36**, 156–162, doi:10.1175/1520-0469(1979)036<0156:SDOPPI>2.0.CO;2.

Jin, Y., and Coauthors, 2014: The impact of ice phase cloud parameterizations on tropical cyclone prediction. *Mon. Wea. Rev.*, **142**, 606–625, doi:10.1175/MWR-D-13-00058.1.

Kessler, E., 1969: *On the Distribution and Continuity of Water Substance in Atmospheric Circulations. Meteor. Monogr.*, No. 32, Amer. Meteor. Soc., 84 pp.

Lamb, D., 2001: Rain production in convective storms. *Severe Convective Storms, Meteor. Monogr.*, No. 28, Amer. Meteor. Soc., 299–321.

Langlois, W. E., 1973: A rapidly convergent procedure for computing large-scale condensation in a dynamical weather model. *Tellus*, **25A**, 86–87, doi:10.1111/j.2153-3490.1973.tb01598.x.

Milbrandt, J. A., and M. K. Yau, 2005: A multimoment bulk microphysics parameterization. Part I: Analysis of the role of the spectral shape parameter. *J. Atmos. Sci.*, **62**, 3051–3064, doi:10.1175/JAS3534.1.

——, and R. McTaggart-Cowan, 2010: Sedimentation-induced errors in bulk microphysics schemes. *J. Atmos. Sci.*, **67**, 3931–3948, doi:10.1175/2010JAS3541.1.

Mlawer, E. J., S. J. Taubman, P. D. Brown, and M. J. Iacono, 1997: Radiative transfer for inhomogeneous atmospheres: RRTM, a validated correlated-k model for the longwave. *J. Geophys. Res.*, **102**, 16 663–16 682, doi:10.1029/97JD00237.

Morrison, H., G. Thompson, and V. Tatarskii, 2009: Impact of cloud microphysics on the development of trailing stratiform precipitation in a simulated squall line: Comparison of one- and two-moment schemes. *Mon. Wea. Rev.*, **137**, 991–1007, doi:10.1175/2008MWR2556.1.

——, S. A. Tessendorf, K. Ikeda, and G. Thompson, 2012: Sensitivity of a simulated midlatitude squall line to parameterization of raindrop breakup. *Mon. Wea. Rev.*, **140**, 2437–2460, doi:10.1175/MWR-D-11-00283.1.

Pruppacher, H. R., and J. D. Klett, 1997: *Microphysics of Clouds and Precipitation*. 2nd ed. Kluwer Academic Publishers, 954 pp.

Reeves, H. D., and D. T. Dawson, 2013: The dependence of QPF on the choice of microphysical parameterization for lake-effect snowstorms. *J. Appl. Meteor. Climatol.*, **52**, 363–377, doi:10.1175/JAMC-D-12-019.1.

Reisner, J., R. M. Rasmussen, and R. T. Bruintjes, 1998: Explicit forecasting of supercooled liquid water in winter storms using the MM5 mesoscale model. *Quart. J. Roy. Meteor. Soc.*, **124**, 1071–1107, doi:10.1002/qj.49712454804.

Rogers, R. R., and M. K. Yau, 1989: *A Short Course in Cloud Physics*. 3rd ed. Pergamon Press, 293 pp + xiv.

Seifert, A., 2008: On the parameterization of evaporation of raindrops as simulated by a one-dimensional rainshaft model. *J. Atmos. Sci.*, **65**, 3608–3619, doi:10.1175/2008JAS2586.1.

——, and K. D. Beheng, 2006: A two-moment cloud microphysics parameterization for mixed-phase clouds. Part 1: Model description. *Meteor. Atmos. Phys.*, **92**, 45–66, doi:10.1007/s00703-005-0112-4.

Skamarock, W. C., and Coauthors, 2008: A description of the Advanced Research WRF version 3. NCAR Tech. Note NCAR/TN-475+STR, 113 pp., doi:10.5065/D68S4MVH.

Straka, J. M., 2011: *Cloud and Precipitation Microphysics: Principles and Parameterizations.* Cambridge University Press, 392 pp.

Thompson, G., P. R. Field, R. M. Rasmussen, and W. D. Hall, 2008: Explicit forecasts of winter precipitation using an improved bulk microphysics scheme. Part II: Implementation of a new snow parameterization. *Mon. Wea. Rev.*, **136**, 5095–5115, doi:10.1175/2008MWR2387.1.

Van Weverberg, K., A. M. Vogelmann, H. Morrison, and J. A. Milbrandt, 2012: Sensitivity of idealized squall-line simulations to the level of complexity used in two-moment bulk microphysics schemes. *Mon. Wea. Rev.*, **140**, 1883–1907, doi:10.1175/MWR-D-11-00120.1.

Verlinde, H., and W. R. Cotton, 1993: Fitting microphysical observations of nonsteady convective clouds to a numerical model: An application of the adjoint technique of data assimilation to a kinematic model. *Mon. Wea. Rev.*, **121**, 2776–2793, doi:10.1175/1520-0493(1993)121<2776:FMOONC>2.0.CO;2.

Wang, Y. Q., 1995: An inverse balance equation in sigma-coordinates for model initialization. *Mon. Wea. Rev.*, **123**, 482–488, doi:10.1175/1520-0493(1995)123<0482:AIBEIS>2.0.CO;2.